

ANALYSIS OF A GAS-PHASE PARTITIONING TRACER TEST
CONDUCTED IN FRACTURED MEDIA

by

Michelle Anne Simon

Copyright © Michelle Anne Simon 2004

A Dissertation Submitted to the Faculty of the

DEPARTMENT OF SOIL, WATER, AND
ENVIRONMENTAL SCIENCE

In Partial Fulfillment of the Requirements
For the Degree of

DOCTOR OF PHILOSOPHY

In the Graduate College

THE UNIVERSITY OF ARIZONA

2004

UMI Number: 3145132

Copyright 2004 by
Simon, Michelle Anne

All rights reserved.

INFORMATION TO USERS

The quality of this reproduction is dependent upon the quality of the copy submitted. Broken or indistinct print, colored or poor quality illustrations and photographs, print bleed-through, substandard margins, and improper alignment can adversely affect reproduction.

In the unlikely event that the author did not send a complete manuscript and there are missing pages, these will be noted. Also, if unauthorized copyright material had to be removed, a note will indicate the deletion.

UMI[®]

UMI Microform 3145132

Copyright 2004 by ProQuest Information and Learning Company.

All rights reserved. This microform edition is protected against
unauthorized copying under Title 17, United States Code.

ProQuest Information and Learning Company
300 North Zeeb Road
P.O. Box 1346
Ann Arbor, MI 48106-1346

The University of Arizona ®
Graduate College

As members of the Final Examination Committee, we certify that we have read the

dissertation prepared by Michelle Anne Simon

entitled Analysis of A Gas-Phase Partitioning Tracer Test

Conducted in Fractured Media

and recommend that it be accepted as fulfilling the dissertation requirement for the

Degree of Doctor of Philosophy

Mark L. Brusseau

Dr. Mark L. Brusseau

1 June 2004

date

Janick M. Ariola

Dr. Janick M. Ariola

5-15-04

date

A. W. Warrick

Dr. A. W. Warrick

5-15-04

date

J. O. L. Wendt

Dr. Jost O. L. Wendt

5-5-04

date

James Farrell

Dr. James Farrell

5-7-04

date

Final approval and acceptance of this dissertation is contingent upon the candidate's submission of the final copies of the dissertation to the Graduate College.

I hereby certify that I have read this dissertation prepared under my direction and recommend that it be accepted as fulfilling the dissertation requirement.

Mark L. Brusseau

Dissertation Director: Dr. Mark L. Brusseau

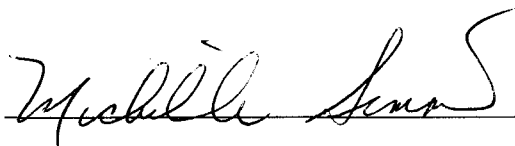
11 June 2004

date

STATEMENT BY AUTHOR

This dissertation has been submitted in partial fulfillment of requirements for an advanced degree at The University of Arizona and is deposited in the University Library to be made available to borrowers under the rules of the library.

Brief quotations from this dissertation are allowable without special permission, provided that accurate acknowledgment of source is made. Requests for permission for extended quotation from or reproduction of this manuscript in whole or in part may be granted by the copyright holder.

SIGNED:  _____

ACKNOWLEDGMENTS

I appreciate all of the funding provided by the United States Environmental Protection Agency. I would like to thank my management for allowing me to pursue this advanced degree, especially Patricia Erickson, Thomas Holdsworth, Teri Richardson, Edward Bates, Dr. Benjamin Blaney, Robert Olexsey and Tim Oppelt. I greatly appreciate the assistance rendered by the United States Air Force, especially Dennis Scott; Tracer Research Corporation, especially Dr. Glenn Thompson, Dr. Randy Golding and Lawrence W. Schenmeyer; and R.E. Wright Inc., especially Peter Cagnetta. This project would not have been possible without the help of The University of Arizona Transport Laboratory personnel, especially, Asami Murao, Malisa Cariño, Greg Schnaar, and Justin Marble. Dr. William Slack's expert Visual Basic Modeling and proofreading skills greatly enhanced this dissertation, as has the technical editorship of Dr. Endakachew Sahle-Demessee. A very special thanks is extended to Etsuko Arita and Dr. Reginald McGinnis, my genial hosts and housemates during my many stays in Tucson. Most of all, I appreciate the patience, tack and expertise of Dr. Mark Brusseau, Ms. Judi Ellwanger, and the members of my dissertation committee for quickly and diligently responding to my ever increasing needs. I wish that all graduate students could have the support, and the fun, that I had during this project.

DEDICATION

To Bill and Marcy - THANKS FOR YOUR PATIENCE!!

As well as,

Mom, Dad, Celeste, Brian, Pat, Lisa, Stephanie, Craig, Mike, Katalina, Kevin, and Dana

TABLE OF CONTENTS

LIST OF ILLUSTRATIONS	7-8
LIST OF TABLES	9-10
LIST OF ACRONYMS	11
ABSTRACT	12
CHAPTER 1. INTRODUCTION	14
CHAPTER 2. LABORATORY METHOD FOR MEASUREMENT OF PARTITION COEFFICIENTS BETWEEN VARIOUS GAS TRACERS AND NON- AQUEOUS PHASE LIQUIDS	18
CHAPTER 3. MEASUREMENT OF HENRY'S LAW CONSTANT FOR GAS PHASE PARTITIONING TRACERS METHODS AND RESULTS	39
CHAPTER 4. ANALYSIS OF A PARTITIONING GAS TRACER TEST CONDUCTED IN AN UNSATURATED FRACTURED CLAY FORMATION	43
CHAPTER 5. USING SIMPLE SPREADSHEET MODELS TO ANALYZE GAS PHASE TRACER TESTS CONDUCTED IN FRACTURED MEDIA	77
CHAPTER 6. CONCLUSIONS	116
REFERENCES	120

LIST OF ILLUSTRATIONS

FIGURE 2.1 Schematic of Equipment Apparatus	30
FIGURE 2.2 Perfluoride Data and Linear Regression	31
FIGURE 2.3 Halon Data and Linear Regression	32
FIGURE 4.1 Tucson International Airport Site Map	71
FIGURE 4.2 Illustration of the stratigraphy and well completion details in a NE-SW direction	72
FIGURE 4.3 Illustration of the stratigraphy and well completion details in a NE-SE direction	73
FIGURE 4.4 VE305D Tracer Concentration Breakthrough Curve versus Time	74
FIGURE 4.5 VM302D Tracer Concentration Breakthrough Curve versus Time	75
FIGURE 4.6 VM301D Tracer Concentration Breakthrough Curve versus Time	76
FIGURE 5.1 Breakthrough Curve and Modeled Results for PDMCB from P8M	110
FIGURE 5.2 Breakthrough Curve and Modeled Results for PDMCB from VM302D.	111
FIGURE 5.3 Breakthrough Curve and Modeled Results for Corrected Ethane from P8M	112
FIGURE 5.4 Breakthrough Curve and Modeled Results for Corrected Ethane from VM302D	113

LIST OF ILLUSTRATIONS, continued

FIGURE 5.5 Breakthrough Curve and Modeled Results for BCF from P8M114

FIGURE 5.6 Breakthrough Curve and Modeled Results for BCF from VM302D115

LIST OF TABLES

TABLE 2.1 Chemical Properties of Trichloroethylene and Tracer Compounds	33-34
TABLE 2.2 Experimental Values for TCE-Air Partition Coefficients	35-36
TABLE 2.3A Average Standard Deviations for Terms in TCE-Air Partition Coefficients Experimental Error Equation (6)	37
TABLE 2.3BAverage Standard Deviations for Terms in TCE-Air Partition Coefficients Experimental Error Equation (6) continued	37
TABLE 2.4 Values for Variance and Percent of Total Variance for Terms in TCE-Air Partition Coefficients Experimental Error Equation (6)	38
TABLE 3.1 Henry's Law Constants at 24 °C	42
TABLE 4.1 Physical and Chemical Information of Gas Tracers	62
TABLE 4.2 Well Completion Information	63-64
TABLE 4.3 TIA Site Permeability Calculations	66
TABLE 4.4 Analysis of Moments - Tucson Airport Site Gas Partitioning Tracer Test	67-68
TABLE 4.5 Saturation Calculations -Tucson Airport Site Gas Partitioning Tracer Test	69
TABLE 4.6 Analysis of S_n Variance	70
TABLE 5.1 Formation Details	99

LIST OF TABLES, continued

TABLE 5.2 Model Details	100-103
TABLE 5.3 Comparison of All Models for PDMCB Inoculated into P8M	104
TABLE 5.4 Comparison of All Models for PDMCB Inoculated into VM302D	105
TABLE 5.5 Comparison of All Models for Ethane Inoculated into PM8	106
TABLE 5.6 Comparison of All Models for Ethane Inoculated into VM302D	107
TABLE 5.7 Comparison of All Models for BCF inoculated into PM8	108
TABLE 5.8 Comparison of All Models for BCF Inoculated into VM302D	109

LIST OF ACRONYMS

BCF	Bromochlorodifluoromethane
DDM	Dibromodifluoromethane
DTE	Dibromotetrafluoroethane
E	Ethane
He	Helium
M	Methane
MCL	Maximum contaminant level
NAPL	Nonaqueous phase liquid
PDMCB	Perfluorodimethylbutane,
PMCH	Perfluoromethylhexane
PMCP	Perfluoromethylpentane
PTT	Partitioning Tracer Test
SG	Specific Gravity
SVE	Soil Vapor Extraction
TCE	Trichloroethylene
TIA	Tucson International Airport
VOC	Volatile Organic Compound

ABSTRACT

This work successfully applied the gas-phase partitioning tracer method to determine the NAPL, water and air saturations in the vadose zone at the field scale. This project was one of the first, and still one of the few, field-scale gas-phase partitioning tracer tests. This work differs from other work in that it was conducted in a high water content, fractured clay.

There were three primary components of this work. First, gas-phase tracers were identified and their NAPL-air and Henry's Law constants measured. There were four types of tracers used in this study: noble gases or nonpartitioning tracers; alkanes, which were expected to be nonpartitioning tracers; perfluorides, NAPL partitioning tracers; and halons, NAPL and water partitioning tracers. A laboratory method for measuring NAPL-air partition coefficients was developed and TCE-air partition coefficients were measured for the perfluoride and halon tracers.

The second component of this study involved conducting a field-scale gas-phase partitioning tracer test, the results which were used to estimate NAPL, water and air saturations. The NAPL saturation, calculated to be an extremely low value, resulted in an estimate of NAPL mass present that is similar to the amount that has subsequently been extracted from the test site via SVE remediation. The alkane tracers, which had been used previously in laboratory column studies as nonpartitioning tracers, were more retarded than the perfluoride tracers at this site. It was the alkane tracers, and not the halon tracers, that were used to determine the water content. The water content was estimated to be approximately 90%, which is unexpectedly high for a vadose zone.

Additionally, the tracer response time, vacuum data, and other geological data indicated that the tracer test was performed in fractured clay.

The third component of this work comprised an analysis of the tracer test data to determine transport parameters. The analysis employed matching eight simple mathematical models to the experimental data. All of the models tested: two porous, three double-porosity, and three fracture-based (single fracture, multifracture, fracture-matrix) models could reasonably match the experimental data and no one model resulted in consistently superior predictions than the others.

CHAPTER 1. INTRODUCTION

Volatile organic compounds (VOCs), especially halogenated VOCs, are some of the most ubiquitous contaminants in the subsurface. The most common method used to remediate VOC contamination in the vadose zone is soil vapor extraction (SVE). SVE can successfully remove thousands of kilograms of VOCs from the vadose zone within one year of operation while groundwater extraction often removes less than hundreds of kilograms after decades. But SVE, like groundwater extraction, does not remove all contaminant mass. In the United States, SVE site closure criteria are determined by modeling the transport of the remaining contaminant mass into the underlying groundwater. The mass flux of the contaminant, when mixed within the saturated zone, must be below the Federal Safe Drinking Water Act maximum contaminant level (MCL). The parties responsible for remediating a contaminate site: the individual State Environmental Protection Agency, and the United States Environmental Protection Agency agree upon a value for the rate of infiltration through the vadose zone, the size and amount of mixing within the groundwater unit, and the methodology for calculating the contaminant mass flux.

Into the 1990's, most of the fate and transport vadose zone infiltration models assumed that the contaminants' concentrations were in local equilibrium between the air and water phases. They could not account for the presence of NAPL phase of the contaminant, should it exist. The presence of NAPL would lengthen the time necessary to remediate

the site and complicate contaminant mass flux modeling. It is difficult to definitively determine NAPL mass by standard methods, such as sampling soil gas or soil.

The concept of partitioning tracer tests (PTTs) was established in the petroleum field to determine residual oil saturates so as to determine enhanced oil recovery economics. In the mid-1990's, several researchers were applying PTT technology to determine the presence and quantity of NAPL for environmental remediation.

This project took place at one of the primary source locations at the Tucson International Airport (TIA) Superfund site. Past practices at this site resulted in high levels of chlorinated VOCs to contaminating approximately 40 meters of vadose zone and groundwater. The primary contaminant of concern is trichloroethylene (TCE). SVE was the decided remedy for the source zone. Several triple completion wells were drilled and attached to air compressors and carbon adsorption units. It was decided to attempt a gas-phase PTT at this site immediately prior to the SVE system start-up (summer of 1996). At the time, the author was aware of only a few field-scale PTTs conducted, and those were conducted only in the saturated zone. In fact, there was one vadose zone PTT test conducted at the Sandia National Laboratory in the late fall of 1995.

This work sought to resolve several questions:

1. Is NAPL present at the TIA site?

2. If so, what is the quantity of NAPL present?
3. If NAPL is present, what is the simplest, yet physically accurate method for modeling contaminant flux?
4. Is PTT technology applicable to the vadose zone?
5. If so, what are suitable gas-phase tracers?
6. What are the necessary NAPL-air and water-air (Henry's Law constants) partitioning coefficients of the selected tracers?
7. What are the applicable field design parameters, e.g., what air flow rates, tracer response times, tracer injection mass, tracer effluent concentrations, etc.?

The results of the studies conducted to address these questions are presented herein.

Three suites of three tracers were injected into three wells 5-10 m distant from a single extraction well. The nine tracer concentrations were measured in the effluent from the extraction well. Geological information of the zone of interest for this work indicated that the tracer injection and extraction would be in a clay with low permeability. The first tracer arrival times were estimated be four hours. However, all tracers were recovered within two hours and it was not possible to analyze the tracer breakthrough curves. Therefore, the same three suites of tracers were then injected into wells 14.5 to 24 m away from the extraction well and this dissertation discusses the second tracer inoculation.

The technique for measuring NAPL-air partition coefficients for gas-phase tracers is described in Chapter 2; the method used to measure their Henry's Law constants is presented in Chapter 3; the description and analysis of the TIA field PTT test are presented in Chapter 4; the attempts to match simple transport models to the data are presented in Chapter 5 and the conclusions of the dissertation work are presented in Chapter 6.

CHAPTER 2. LABORATORY METHOD FOR MEASUREMENT OF PARTITION COEFFICIENTS BETWEEN VARIOUS GAS TRACERS AND NON-AQUEOUS PHASE LIQUIDS

Introduction

Partitioning tracer tests are used to identify the presence and quantify the amount of non-aqueous phase liquid (NAPL) present in the subsurface, (cf. Jin et al. 1995; Wilson and Mackay 1995; Nelson and Brusseau 1996; Rao et al. 1997; Falta et al. 1999; Cain et al. 2000). In a partitioning tracer test, a pulse containing two or more tracers is injected into the subsurface and samples collected from a location distant from the injection points are analyzed for tracer concentrations. If one compound preferentially separates from the flowing stream into an immobile, immiscible liquid, then its arrival at the extraction points is delayed. The magnitude of this delay has been correlated to the amount of immiscible liquid present (Tang 1992). Accurate knowledge of the quantity of NAPL present in the subsurface can assist in remedial process selection and optimization, as well as the development of closure criteria. While it is more common to perform tracer partitioning experiments in the saturated zone, vadose zone gas tracer experiments have been performed (Simon et al. 1998; Mariner et al. 1999; Brusseau et al. 2003; Keller and Brusseau 2003).

In a vadose zone contaminated with an immiscible chlorinated compound, there are three fluid phases present: gas, water and NAPL. The procedure for calculating the amount of

NAPL present, involves the calculation of the retardation factor (Brusseau et al. 2003a):

$$R_i = \frac{t_p}{t_c} = 1 + \frac{S_w}{K_H S_g} + \frac{K_D \rho_b}{\theta K_H S_g} + K_N \frac{S_n}{S_g} \quad (1)$$

where the retardation factor, R_i [dimensionless], is computed as the ratio of t_p [cm/sec], the mean travel time for the partitioning tracer, to t_c [cm/sec], to the mean travel time for the partitioning tracer. Further analysis shows that this quotient of travel time is related, as shown in equation (1), where S_w is the water saturation, [dimensionless]; S_g is the gas saturation, [dimensionless]; S_n is the NAPL saturation, [dimensionless]; K_H is the gas-water partition coefficient, [Henry's Law Constant, dimensionless]; K_D is the soil-water partition coefficient, [mL/g]; K_N is NAPL-air partition coefficient, [dimensionless]; θ is the total porosity [dimensionless]; and ρ_b is soil bulk density, [g/mL]. Specifically, the dimensionless saturations (S_w , S_n and S_g) are the fractional volume of pore space occupied by the respective phase. The partition coefficient, K_i , of a substance is the ratio of the concentration of the substance in one phase to the concentration of the substance in another. Each partition coefficient in equation (1) is defined in equation (2):

$$K_H = \frac{C_g}{C_w}; \quad K_D = \frac{C_s}{C_w}; \quad K_N = \frac{C_n}{C_g} \quad (2)$$

where C_g is the concentration in the gas phase, [g/mL]; C_w is concentration in the water

phase, [g/mL]; C_n is concentration in the NAPL phase, [g/mL]; and C_s is the sorbed mass fraction, [dimensionless] (Brusseau et al. 2003a).

Given accurate values of partition coefficients, a trio of retardation factors generated by three tracers can be manipulated via equation (1) to yield saturation values of the gas, water and NAPL. Despite the difficulties commonly encountered in measuring retardation factors, the quality of the partition coefficient dominates these calculations (Deeds et al. 1999b). While the Henry's Law constants, K_H , for many compounds are well known (e.g. Mackay and Shiu 1981) and K_D has been correlated to octanol-water coefficients (e.g., Karickhoff 1984), the NAPL-air partition coefficients, K_N , are sparsely documented. It is the goal of this work to measure the NAPL-air partition coefficients for selected compounds.

Whitley (1997) describes an empirical method for measuring gas tracer partition coefficients via transport of retarded and nonretarded tracers through a column with known concentrations of water and NAPL. The NAPL-air partition coefficients are calculated from analysis of the breakthrough curves. The method used in this study differs from Whitley's method in that a known mass of tracer compound is introduced into a vial containing known masses of NAPL and air. This method, as was the method used for aqueous tracers in Dugan et al. (2003), is more similar to the methods for calculating Henry's Law constants and shares the advantage of being straightforward and

rapidly executed. The method developed through this study requires accurate measurements of vapor compositions, vial size, inoculated tracer mass, tracer density, NAPL mass, and NAPL density. The tractable equation used to process the measurements allows for the relative importance of component measurements.

Materials and Equipment

For this study, trichloroethylene (TCE), a common contaminant at many sites on the National Priority List, was chosen as a representative NAPL compound. The chemicals used in this study, aliases, CAS numbers, and related chemical properties are presented in Table 1. The compounds, perfluorodimethylcyclobutane (PFDMB), perfluoromethylcyclopentane (PFMP), perfluoromethylcyclohexane (PFMH), dibromodifluoromethane (DDM), and dibromotetrafluoroethane (DTE), were selected because they were used in a vadose zone partitioning tracer test (Simon et al. 1998). The perfluoride tracers, PFDMB, PFMP, and PFMH, partition significantly into NAPL but minimally into water. The halon tracers (DDM and DTE) partition into both water and NAPL.

The equipment for this study consisted of several 20-mL vials (Kimble Co., Vineland, NJ), 1-mL syringes (Terumo, Elkton, MD), 10 μ L syringes (Hamilton Model 701, Reno, NV), 10,000- μ L syringes (MicroMate, Popper & Sons, New Hyde Park, NJ), and an AE200 Mettler Balance (Mettler Toledo, Columbus, OH). A thermometer (Fisherbrand,

Middleton, Manchester, UK) was used to measure system temperatures. A Hewlett-Packard HP 5890 Series II Gas Chromatograph (GC) equipped with an electron capture detector (ECD) and Series II Integrator were used to measure tracer gas concentrations.

Methodology

These experiments were conducted at ambient temperatures and pressures, which were recorded. The exact volume of each of 20-mL vials were determined via weighing them empty, filling them with water, reweighing them, and then drying them before use. Two, three, five, or six mL of TCE were placed into 20-mL vials, in duplicate; capped; and weighed. Then, approximately 0.2 g of tracer material, as a neat liquid, was injected into the TCE-air laden vials via a disposable 1-mL syringe. Then, the TCE-air-tracer laden vials were reweighed. The tracer materials were stored in a freezer at -15 °C so that they were in a liquid state when they were injected. Nevertheless, the liquid tracers were very volatile. Needles and the syringes that were used to inoculate the tracer into the TCE-laden vials, were placed in a freezer prior to use to minimize the volatilization of the tracers as they were inoculated into the vial. Even with these precautions, it was not possible to inoculate duplicate quantities of tracer into the eight vials because of the volatility of the tracer compounds. The TCE-air-tracer laden vials were agitated on a shaker table for ten minutes before chromatographic analysis.

For performing Henry's Law constant measurements, a 30 minute equilibration period is

sufficient according to Peng and Wan (1997). Since this method relies on mass balances, all TCE-air partition coefficient measurements were performed within eight hours of mixing the TCE and tracer compound to minimize mass loss via leakage. The average weight loss after the vials were reweighed after analyses was 0.0025 g for this study, or 0.01% of the average total vial weight. Gossett (1987) reported that the vials would leak less if stored in the inverted position, so all vials were placed in the inverted position. The vials were gently shaken for 30 seconds and then allowed to sit undisturbed for 90 seconds immediately prior to analyses in order to homogenize the vapor phase in the vial.

After equilibrium had been established, a 10- μ L aliquot of headspace was collected via a new 10- μ L syringe and injected into a 10,000- μ L syringe filled with 5000 μ L of nitrogen and equipped with a stopper in the needle. After five minutes and using a new 10- μ L syringe, a 7- μ L aliquot was collected from the first 10,000- μ L syringe and placed into a second 10,000- μ L syringe filled with 5000 μ L of nitrogen and equipped with a stopper in the needle. The plunger of the 10- μ L syringe was pushed and pulled five times into the 10,000- μ L syringes to increase mixing. See Figure 1.

Due to the high concentrations of the free-phase TCE and tracer headspace concentrations, a two-step dilution was necessary. Tracer concentrations in the first aliquot from the second 10,000- μ L syringes were consistently higher than subsequent

samples as sampling introduced air. Therefore, that value, rather than the average value of two or more aliquots, was used for the calculations. Since it was not possible to decontaminate the 10- μ L syringes due to the high concentrations of the TCE and tracer in the headspace, all 10- μ L syringes could be used only once. The 10,000- μ L syringes were baked in a 190 °C oven for at least two hours between uses to prevent cross contamination.

Results and Discussion

The tracer concentration in the liquid phase can be determined from a mass balance:

$$C_n = \frac{M_{To} - C_g V_g}{V_n} \quad (3)$$

where M_{To} is mass of tracer initially injected into the vial, [μ g]; C_g is concentration of tracer in vapor phase at equilibrium, [μ g/mL]; C_n is concentration of tracer in NAPL phase at equilibrium, [μ g/mL], V_g is volume of vapor phase, [mL]; V_n is volume of NAPL phase, [mL]. The concentration of the tracer in the liquid TCE phase was not directly measured.

The partition coefficients measured from this work are presented in Table 2. The TCE-air partition coefficients for gas tracer compounds PDMCB, PMCP, PMCH, DDM, and DTE were calculated to be 22, 24, 53, 370 and 470, respectively for ambient temperatures.

The values for the partition coefficients were determined by calculating the ratio of the tracer concentration in the liquid to the vapor phase for eight different vials per compound. The partition coefficient was also calculated as the slope of a linear plot of vapor concentration versus liquid concentration. Plotting C_g versus C_n produced correlation coefficients ranging from 0.49 to 0.98 (Figures 2-3). The partition coefficients measured in study were higher than those measured by Whitley (1997) by 34-43% but may have been measured at higher temperatures than those by Whitley, which were not reported. Nevertheless, this methodology produces results consistent with literature values obtained from column tests with satisfactory reproducibility.

There are four critical measurements needed to determine the partition coefficient: mass of tracer introduced into the vial, mass of NAPL introduced into the vial, concentration of the tracer in the vapor phase of the vial, and the determination of the total vial volume. Additionally, the volume of the liquid phase in the vial is determined from the known liquid density of the NAPL and assuming complete miscibility of the tracer into the NAPL. Noting that ρ_N is density of the NAPL, [g/mL]; V_b is vial volume, [mL]; M_N is the mass of NAPL in liquid phase in vial, [g], and the volume of the NAPL phase, $V_n = M_N/\rho_N$; then volume of the gas phase is $V_g = V_b - V_n = V_b - M_N/\rho_N$. Therefore, the mass balance for the tracer injected into each vial can be manipulated to yield an expression for the concentration in the liquid NAPL phase that involves only known masses, volumes, and vapor phase concentrations.

$$C_n = \frac{M_{To}\rho_n}{M_N} - \frac{C_g V_b \rho_N}{M_N} + C_g \quad (4)$$

$$K_{ng} = \frac{M_{To}\rho_N}{C_g M_N} - \frac{\rho_N V_b}{M_N} + 1 \quad (5)$$

In general, the statistical variance of a dependent variable is determined by the variance of the independent variables and the partial derivatives of the dependent variable. The variance of the NAPL-air partition coefficient was derived from Equation (5) using a first-order Taylor series approximation of the variance (Gossett 1987):

$$\begin{aligned} \sigma^2(K_{ng}) = & \left(\frac{\partial K_{ng}}{\partial M_{To}} \right)^2 \sigma^2(M_{To}) + \left(\frac{\partial K_{ng}}{\partial \rho_N} \right)^2 \sigma^2(\rho_N) \\ & + \left(\frac{\partial K_{ng}}{\partial C_g} \right)^2 \sigma^2(C_g) + \left(\frac{\partial K_{ng}}{\partial M_N} \right)^2 \sigma^2(M_N) + \left(\frac{\partial K_{ng}}{\partial V_b} \right)^2 \sigma^2(V_b) \end{aligned} \quad (6)$$

Each of the partial differential terms is equal to:

$$\left(\frac{\partial K_{ng}}{\partial M_{To}} \right) = \frac{\rho_n}{C_g M_N} \quad (7)$$

$$\left(\frac{\partial K_{ng}}{\partial \rho_N} \right) = \frac{M_{To}}{C_g M_N} - \frac{V_b}{M_N} \quad (8)$$

$$\left(\frac{\partial K_{ng}}{\partial C_g} \right) = - \frac{\rho_N M_{To}}{M_N C_g^2} \quad (9)$$

$$\left(\frac{\partial K_{ng}}{\partial V_b} \right) = - \frac{\rho_N}{M_N} \quad (10)$$

$$\left(\frac{\partial K_{ng}}{\partial M_N} \right) = - \frac{\rho_N M_{To}}{C_g M_N^2} + \frac{\rho_N V_b}{M_N^2} \quad (11)$$

The TCE density ranged from 1.463 to 1.454 for the temperature range of 22 to 27 °C (Montgomery 1996); the TCE density standard deviation was calculated to be 4.2×10^{-3} g/mL. Additional measurements were performed to determine the standard deviations for all of the other parameters (Table 3). The standard deviation for the concentration of the tracer in the vapor phase was a function of the calibration procedures and ranged between 9×10^{-6} and 3×10^{-4} g/mL for the five compounds. The standard deviation of the mass measurements is a reflection of the precision of the balances used during this work and was determined to be 5×10^{-4} g. It was not a function of the liquid measured. The standard deviation in water density, which might arise due to variations in technique or temperature, was measured to be 1×10^{-2} g/mL. The variance of both mass measurement and liquid density contributed to the expected variance of the vial volume. By use of a functional relationship similar to equation (6), the variance of vial volume was derived

using a first order Taylor series approximation of the variance:

$$\begin{aligned}\sigma^2(V_b) &= \left(\frac{\partial V_b}{\partial M_w}\right)^2 \sigma^2(M_w) + \left(\frac{\partial V_b}{\partial \rho_w}\right)^2 \sigma^2(\rho_w)^2 \\ &= \left(\frac{1}{\rho_w}\right)^2 \sigma^2(M_w) + \left(\frac{-M_w}{\rho_w^2}\right)^2 \sigma^2(\rho_w)\end{aligned}\quad (12)$$

The standard deviation for the volume vial, the square root of Equation (12) was calculated to be 2.8×10^{-2} mL.

The most significant source of variance for the partition coefficients, as calculated by Equation (6), was related to the measurement of tracer in the vapor phase, C_g , accounting for 99% of the variance. The relative percent difference, $(100\% * \text{standard deviation} / \text{arithmetic average})$, ranged from 8.5 to 25% for these measurements. The variance of the slope from these plots can be compared to those calculated from the data and Equation (6), as per Table 4. The variance in the measurements of TCE-air partition coefficients are consistent among the three methods.

Conclusions

In summary, a relatively simple laboratory method for measuring NAPL-air partition coefficients was developed. The method developed through this study is reproducible

and similar to the methods developed for measuring Henry's Law constants. Most of the variability is due to the uncertainty of measuring tracer vapor phase concentrations with overall relative percent differences ranging from 8.5 to 25%. The uncertainty for partitioning tracer tests to accurately quantify NAPL volumes in the subsurface will be a function of the NAPL-air partition coefficient values, as well as well as other parameters, such as measurement of tracer concentrations in the effluent, potential mass-transfer constraints, and nonuniform formation volumetric sweep.

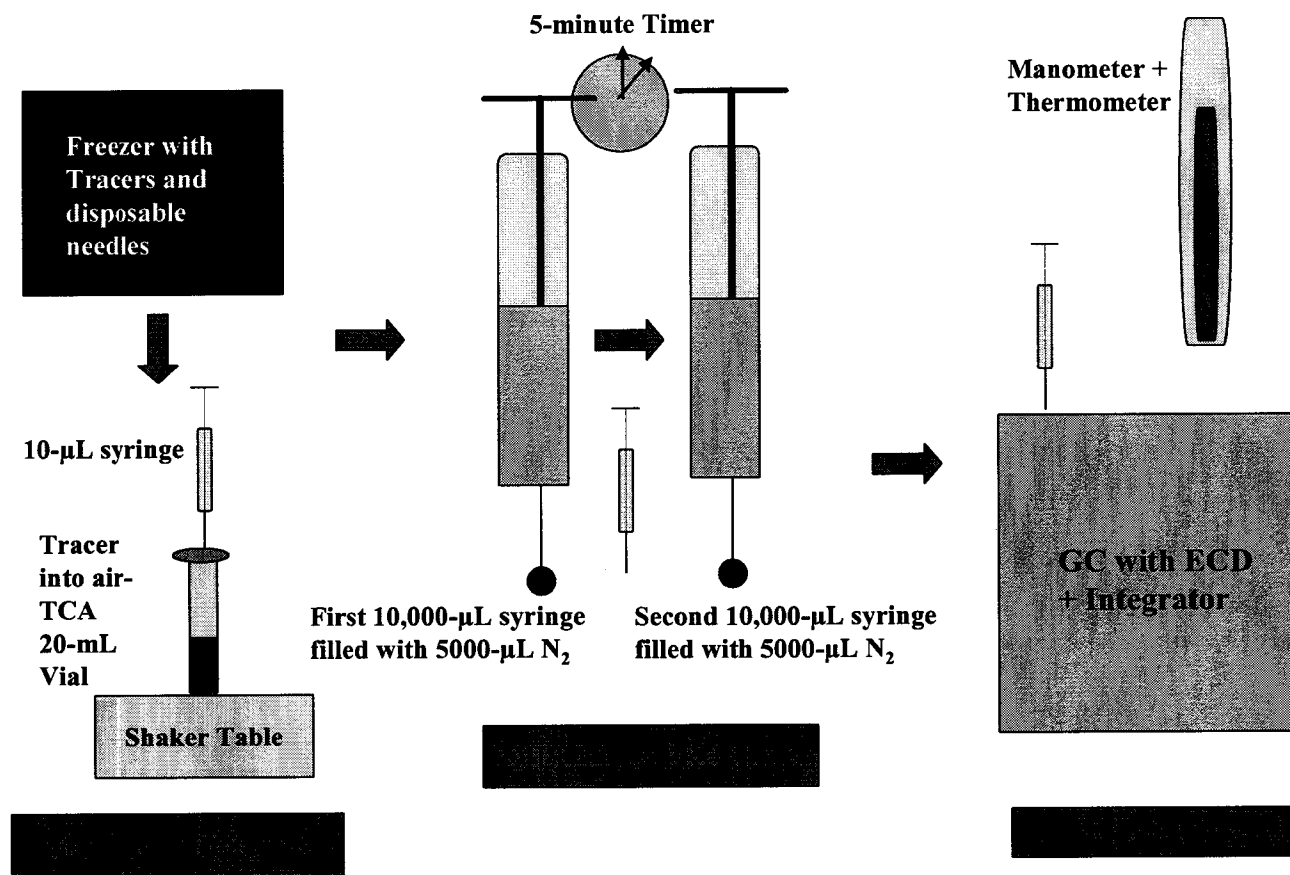


Figure 2.1 Schematic of Equipment Apparatus

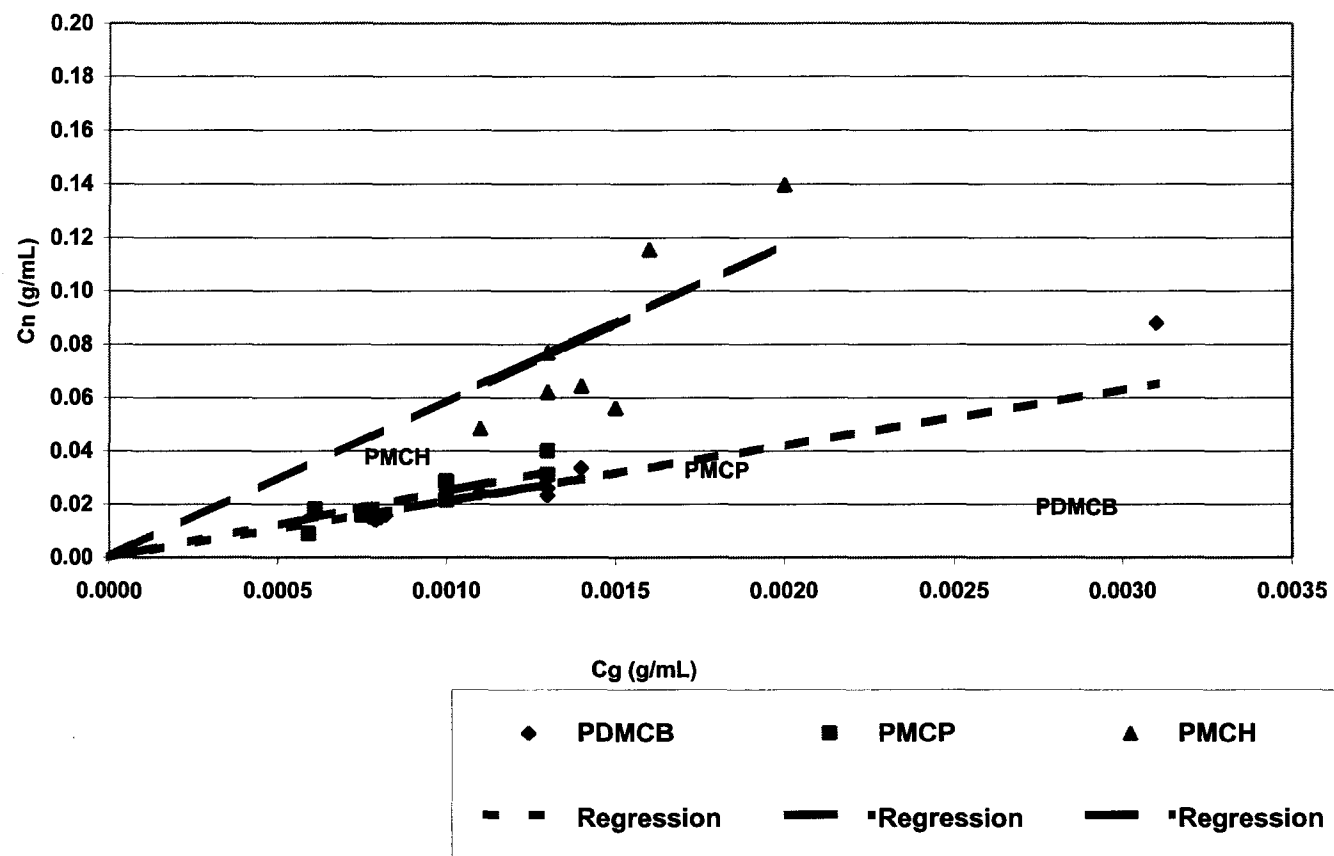


Figure 2.2 Perfluoride Data and Linear Regression

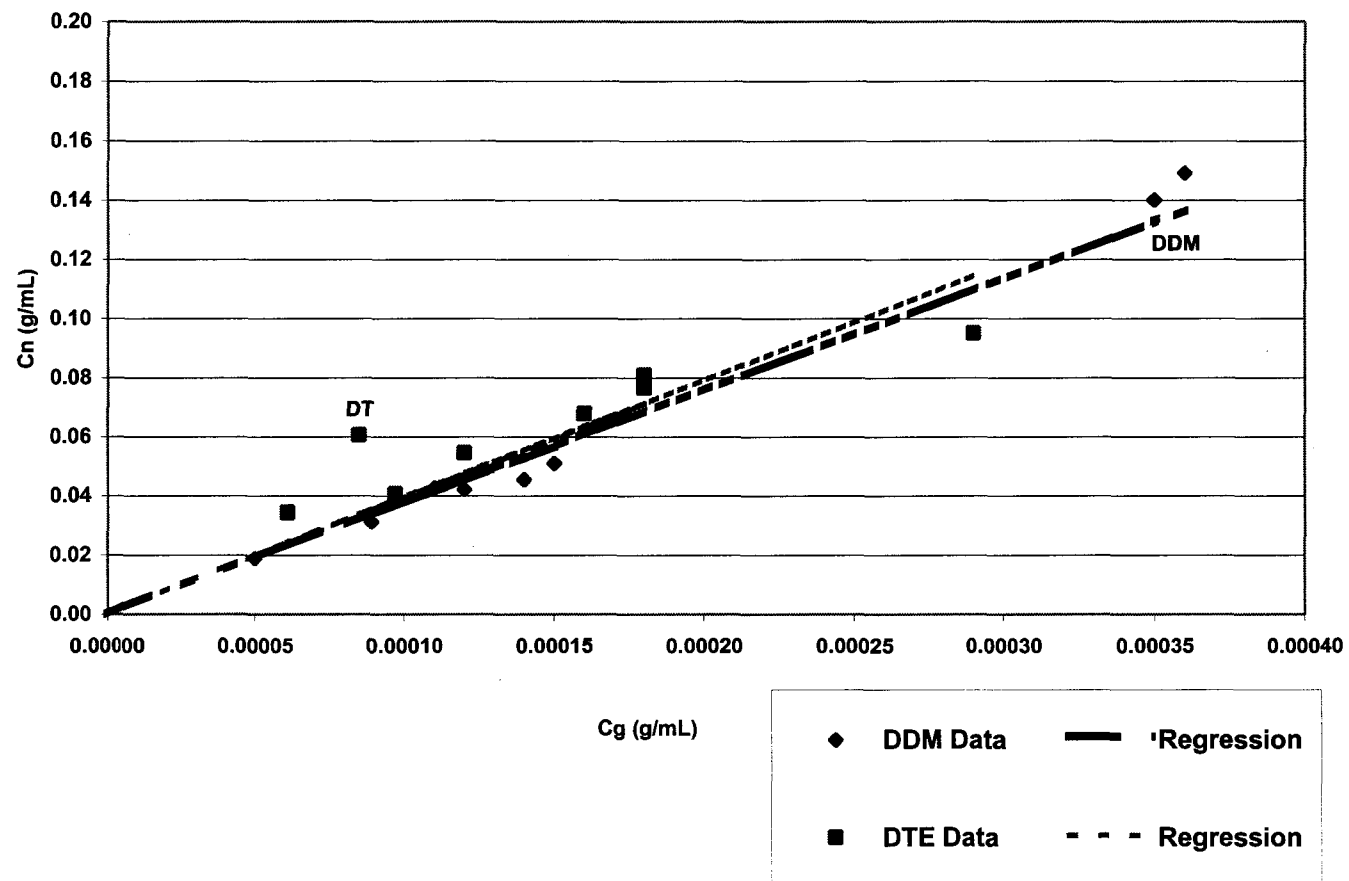


Figure 2.3 Halon Data and Linear Regression

<p>Table 2.1 Chemical Properties of Trichloroethylene and Tracer Compounds</p>							
Compound (Alias)	CAS Number	Formula	Source (purity)	Molecular Weight (g/gmole)	Molecular Volume (L/g) ^f	Liquid Density (g/mL) @ 25 °C	Vapor Pressure (mm Hg)
Trichloroethylene (TCE)	79-01-6	C ₂ HCl ₃	Aldrich (99.5%)	131.5	5.381	1.464 ^s	20 @ 0 °C ^a 57.8 @ 20 °C ^b 75 @ 25 °C ^a 200 @ 50 °C ^a
Perfluorodimethylcyclobutane (PDMCB)	2994-71-0	C ₆ F ₁₂	DuPont (97%)	300	12.277	1.672 ^e	977 @ 25 °C ^c 1060 @ 54.4 °C ^c
Perfluoromethylcyclopentane (PMCP)	180-22-7	C ₆ F ₁₂	Rhône- Poulenc (99 %)	300	12.277	1.707 ^e	368 @ 25 °C ^c
Perfluoromethylcyclohexane (PMCH)	355-02-2	C ₇ F ₁₄	Rhône- Poulenc (99 %)	350	14.323	1.788 ^e	106 @ 25 °C ^d
Dibromodifluoromethane (DDM)	75-61-6	CBr ₂ F ₂	Great Lakes Chemical (99 %)	209.8	8.586	2.306 ^e	652 @ 21 °C ^c
Dibromotetrafluoroethane (DTE)	124-73-2	C ₂ Br ₂ F ₄	Great Lakes Chemical (99.9 %)	259.8	10.632	2.149 ^e	284 @ 25 °C ^c

Table 2.1 Footnotes

a <http://www.icknowledge.com/glossary/t.html>

b <http://www.epa.gov/OGWDW/dwh/t-voc/trichlor.html>

c MSDS sheet

d Synquest Fluorochemicals

e Tracer Research

f Lyman p19-3 $\rho_v = PM/RT$, $R = 0.082 \text{ atm-L/mol-K}$, $P = 1 \text{ atm} = 760 \text{ mm Hg}$, $T = 25 \text{ C} = 298 \text{ K}$

g Montgomery 1996

<p>Table 2.2 Experimental Values for TCE-Air Partition Coefficients</p>								
Compound Alias	K _{ng} Literature Value	No. of Data Pairs	K _{ng} Experimental Arithmetic Average Value + 95% Confidence Limit ^c	K _{ng} Experiment al Range of Values	K _{ng} Experimental Relative Percent Difference (RPD %) ^b	Linear Regression Slope of C _g vs C _n Curve + 95% Confidence Limit ^d	Slope of C _g vs C _n Curve Correlation Factor (r ²)	Experimental Temperature °C
PDMCB	14.7 +/- 3.0 ^a	8	22. +/- 2.5	18. - 28.	17%	21. +/- 2.7	0.79	22-23
PMCP	not available	8	24. +/- 3.9	15. - 31.	23%	25. +/- 2.9	0.79	21-22
PMCH	44 ^a	8	53. +/- 8.7	38. - 72.	24%	59. +/- 9.3	0.71	27-28
DDM	not available	8	370 +/- 22.	330 - 410	8.5%	380 +/- 13.	0.98	26-28
DTE	not available	8	470 +/- 81.	330 - 710	25%	400 +/- 42	0.49	26-28

Table 2.2 Footnotes

^a (Whitley 1997)

^b RPD = 100 *standard deviation/arithmetic average

^c The 95% confidence interval for the eight experimental data pairs = +/- 1.96 * (standard deviation)/(square root of the number of the experimental pairs).

The standard deviation of the experimental pairs = $\sqrt{\frac{n\sum x^2 - (\sum x)^2}{n(n-1)}}$

^d The 95% confidence interval for linear regression of the eight pairs of C_g versus C_n = +/- 1.96 * (standard deviation)/(square root of the number of the experimental

pairs). The standard deviation of the slope of linear plot = $\sqrt{\frac{\frac{\sum (Cn_i - Cn_{predicted})^2}{(n-1)}}{\sum (Cg_i - \bar{Cg})^2}}$. It was assumed that the intercept was zero.

Table 2.3A Average Standard Deviations for Terms in TCE-Air Partition Coefficients Experimental Error Equation (6)					
Compound Alias	$\frac{\partial K_{ng}}{\partial M_{To}}$ (1/g)	$\frac{\partial K_{ng}}{\partial \rho_n}$ (1/g/mL)	$\frac{\partial K_{ng}}{\partial C_g}$ (1/g/mL)	$\frac{\partial K_{ng}}{\partial V_b}$ (1/mL)	$\frac{\partial K_{ng}}{\partial M_n}$ (1/g)
PDMCB	2.4×10^2	1.4×10^1	-2.2×10^4	-3.1×10^{-1}	-4.6×10^0
PMCP	3.5×10^2	1.6×10^1	-3.4×10^4	-3.1×10^{-1}	-5.2×10^0
PMCH	2.2×10^2	3.6×10^1	-4.1×10^4	-3.1×10^{-1}	-1.1×10^1
DDM	2.1×10^3	2.5×10^2	-3.1×10^6	-3.1×10^{-1}	-7.8×10^1
DTE	2.5×10^3	3.2×10^2	-4.4×10^6	-3.0×10^{-1}	-9.6×10^1

Table 2.3B Average Standard Deviations for Terms in TCE-Air Partition Coefficients Experimental Error Equation (6)					
Compound Alias	$\sigma(M_{To})$ (g)	$\sigma(\rho_n)$ (g/mL)	$\sigma(C_g)$ (g/mL)	$\sigma(V_b)$ (mL)	$\sigma(M_n)$ (g)
PDMCB	$5. \times 10^{-4}$	4.2×10^{-3}	1.5×10^{-4}	2.8×10^{-1}	$5. \times 10^{-4}$
PMCP	$5. \times 10^{-4}$	4.2×10^{-3}	1.5×10^{-4}	2.8×10^{-1}	$5. \times 10^{-4}$
PMCH	$5. \times 10^{-4}$	4.2×10^{-3}	3.0×10^{-4}	2.8×10^{-1}	$5. \times 10^{-4}$
DDM	$5. \times 10^{-4}$	4.2×10^{-3}	$9. \times 10^{-6}$	2.8×10^{-1}	$5. \times 10^{-4}$
DTE	$5. \times 10^{-4}$	4.2×10^{-3}	$2. \times 10^{-5}$	2.8×10^{-1}	$5. \times 10^{-4}$

<p>Table 2.4</p> <p>Values for Variance and Percent of Total Variance for Terms in TCE-Air Partition Coefficients</p> <p>Experimental Error Equation (6)</p>								
Compound Alias	Variance due to M_{To}	Variance due to ρ_N	Variance due to C_g	Variance due to V_b	Variance due to M_N	Total Variance as per Eqn (6)	Experimental Variance from Data points	Experimental Variance from C_g vs C_n Slope
PDMCB	1.6×10^{-2}	3.6×10^{-3}	1.2×10^1	9.0×10^{-3}	6.9×10^{-6}	12	13	15
PMCP	4.1×10^{-2}	4.5×10^{-3}	2.9×10^1	8.9×10^{-3}	9.4×10^{-6}	29	31	17
PMCH	1.4×10^{-2}	2.3×10^{-2}	1.5×10^2	9.1×10^{-3}	3.95×10^{-5}	150	160	180
DDM	1.35×10^0	1.1×10^0	1.1×10^3	8.9×10^{-3}	1.9×10^{-3}	1100	970	370
DTE	2.0×10^0	1.9×10^0	1.1×10^4	8.8×10^{-3}	2.7×10^{-3}	11,000	14,000	3,600

CHAPTER 3. MEASUREMENT OF HENRY'S LAW CONSTANT FOR GAS- PHASE PARTITIONING TRACERS METHODS AND RESULTS

This chapter outlines the methodology used to measure the Henry's law constants for the tracers used in the field experiment. It was decided to attempt to measure the Henry's constants of PDMCB, PMCP, PMCH, DDM and DTE. It has not been possible to obtain any BCF compound to date as Tracer no longer uses the compound and its Henry's Law constant is available in the literature. It also was decided not to measure the Henry's Law constants of methane or ethane, as their Henry's Law Constants are well-known. Therefore, it was decided to measure the Henry's Law Constant of trichloroethene (TCE Sigma-Aldrich CAS #79-01-6) in order to compare the results of this technique to literature values.

Methodology for the Determination of Henry's Law Constants

1. Determine the exact volume of numbered 20-mL vials (VMR Catalogue #66011-110) and their aluminum caps and teflon lined septa (VMR Catalogue #66030-794) by weighing vial via Mettler Balance Model AE240, then covered by a numbered cap, and, then filled with nanopure water and weigh vial, cap and water. Empty water and allow to dry in 115 °C oven for over eight-hours. Allowed vials to cool for more than one hour.
2. Place 5 or 10 mL nanopure water into vials, cap and reweigh.
3. Inject, via disposable 1-mL syringe, as close to 0.4 g of tracer as a neat liquid as possible, reweigh. The tracers were extremely volatile and some of the tracer mass

evaporated during the initial injection process. All tracer injections were performed under a laboratory hood. The 1-mL disposable syringes were chilled in the freezer for the TCE-air partition coefficient measurement experiments.

4. Shake on shaker table for 10 min.

5. Collect a 10 μ L aliquot via 10- μ L Hamilton Model 701 syringe of headspace and inject to Hewlett-Packard HP 5890 Series II Gas Chromatograph (GC) equipped with an electron capture detector (ECD) and HP Series II Integrator. The GC was operated at a constant 110 °C temperature. Three or more aliquots of the vapor phase were collected and analyzed via the GC for each vapor measurement.

6. Collect a 5 μ L aliquot via 10- μ L Hamilton Model 701 syringe of liquid phase and inject to Hewlett-Packard HP5890 Series II Gas Chromatograph (GC) equipped with an electron capture detector (ECD) and HP Series II Integrator. The GC was operated at a constant 110 °C temperature. Three or more aliquots of the liquid phase were collected and analyzed via the GC for each liquid measurement.

The 10- μ L Hamilton Model 701 syringes were cleaned between injections by pulling 5 pore volumes of water through the syringe, followed by 5 pore volumes of ethanol. Then the syringe was placed into the FID port of the GC and warm nitrogen was allowed to flow through the syringe for 5 seconds. The 10- μ L Hamilton Model 701 syringe is not a gas tight syringe. Therefore, a small quantity of nanopure water was pulled through the syringe to prevent vapors from leaking through the syringe. Five different 10- μ L Hamilton Model 701 syringes were used to measure Henry's Law constants.

7. Calculate the Henry's Law Constant by dividing average concentration of tracer in headspace (C_g) by average concentration of tracer in water phase (C_w) per vial. The results are listed in Table 3.1. It was not possible to obtain reproducible measurements of the three perfluoride tracers (PDMCB, PMCP and PMCH) in the water phase as all tracer immediately partitioned into any vapor phase that was present, even if it were a small bubble in an otherwise completely water-filled vial. Therefore, it was concluded that these compounds are essentially water insoluble and no further attempts were made to quantify a Henry's Law constant for the perfluoride compounds.

The Henry's Law constants for DDM, DTE and TCE were measured to be 2.94, 11.75 and 0.485, respectively and these values are close to those obtained from the literature (See Table 3.1). Henry's law constants higher than 1, as they are for DDM and DTE, indicate that the majority of the mass of the tracer will be in the vapor, as opposed to the liquid phase. Henry's law constants equal to 0.5, which is approximately the value determined for TCE, indicates that the compound is present at twice the concentration in the aqueous phase as in the vapor phase. The relative percent difference (RPD) for these compounds were somewhat high, 9 to 27, but are approximately the same as the RPD between the three TCE literature values (11%).

Table 3.1 Henry's Law Constants at 24 °C							
Compound	Reference Value	Average	Min	Max	Standard Deviation	RPD ⁶	Count ⁷
DDM	1.55 ¹	2.94	2.66	3.43	0.26	9	6
DTE	3.44 ²	11.75	7.46	16.1	2.99	27	6
TCE	0.392 ³ , 0.479 ⁴ , 0.471 ⁵	0.485	0.33	0.55	0.090	19	5

1. (Nelson et al. 1999a)

2. Estimated from Thermodynamic properties

3. (Gossett 1987)

4. (Hine and Mookerjee 1975)

5. (Ashworth et al. 1988)

6. RPD = 100*standard deviation/average of the number of vials.

7. The count refers to the number of vials of water and tracer compounds. Three or more aliquots of each vial's vapor and liquid phase were collected and analyzed via the GC/ECD.

CHAPTER 4. ANALYSIS OF A PARTITIONING GAS TRACER TEST CONDUCTED IN AN UNSATURATED FRACTURED CLAY FORMATION

Introduction

In a partitioning tracer test (PTT), a pulse containing two or more substances is injected into the subsurface, and samples collected from location(s) distant from the injection points are analyzed for tracer concentrations. If one compound preferentially separates from the flowing stream into immobile, immiscible liquids, then its arrival at the extraction points is delayed. The magnitude of this delay has been correlated to the amount of immiscible liquid present (e.g., Tang 1992). Accurate knowledge of the quantity of NAPL present in the subsurface can assist in remedial process selection and optimization, as well as the development of closure criteria.

This technique is not without precedence; the oil industry has used partitioning tracers for determining oil saturations since the 1970's (Deans 1978; Senum et al. 1992; Tang and Harker 1991). More recently, partitioning tracers have been used to determine NAPL volumes for hazardous waste sites (e.g., Jin et al. 1995; Nelson and Brusseau 1996; Annable et al. 1998) to support environmental restoration. The majority of the work has been performed in the saturated zone, but some work has also been performed in the unsaturated zone (Mariner et al. 1999; Deeds et al. 1999b; Brusseau et al. 2003a; Keller and Brusseau 2003).

Brusseau et al. (1997) achieved success using gas phase tracers for measuring soil water saturations for laboratory columns. Later, lysimeter tests (Nelson et al. 1999a; Carlson et al. 2003) and field-scale studies supported the success of PTT for measuring water saturations (Deeds et al. 1999a; Keller and Brusseau 2003). Field-scale unsaturated zone PTTs were also used to determine the NAPL saturations (Deeds et al. 1999b; Mariner et al. 1999; Brusseau et al. 2003a) in relatively homogeneous media. Additional efforts have addressed a variety of complicating factors. Brusseau et al. (1998); Nelson et al. (1999); Meinardus et al. (2002), and Johnson et al. (2003) investigated the effects of a heterogeneous formation on the interpretation of partitioning tracers. Brusseau et al. (1997), Costanza and Brusseau (2000), Costanza-Robinson (2001) and Kim et al. (2001) quantified the retention effects of tracer partitioning to the air-water interface. Semprini et al. (2000) attempted to quantify the presence of NAPL to reduction in the concentration of naturally occurring radon-222. Davis et al. (2002) furthered the technique measuring the reduction of naturally occurring radon-22 with a single well push-pull test. While most tests involve advective flow, there have been several diffusive partitioning tracer tests have been performed as well (Vulava et al. 2002; Werner and Hohener 2002).

The value of utilizing a tracer test to obtain hydrogeological and transport parameters has been documented (Jin et al. 1997; Zhang and Graham 2001; and Brusseau et al. 2003b). Johnson et al. (2003) measured diffusion coefficients at the field-scale. Meinardus et al. (2002) compared partitioning tracer NAPL volume estimates to high density core data.

Kram et al. (2001) compared several methods of DNAPL characterization methods.

Keller and Brusseau (2003) successfully compared water saturations values calculated by partitioning tracer tests to those values determined by gravimetric core analysis, neutron scattering and bore-hole ground penetrating radar.

This work describes an early vadose zone gas partitioning test performed at a contaminated site in Tucson, Arizona. Analysis of the PTT data allowed the authors to develop a comprehensive conceptual site model.

Theory

There are only two phases present in the saturated zone, water and NAPL, and there is a binary system for interpreting partitioning tracer response. In the unsaturated zone there are three phases: air, water and NAPL, and therefore at least three types of gas tracers are needed. In fact, four types of gas-phase partitioning tracer types have been identified: (1) nonpartitioning, nonsorbing tracers, (2) primarily NAPL partitioning, (3) primarily water partitioning and (4) NAPL and water partitioning. Noble gases such as helium, argon, neon, and krypton are examples of commonly used nonpartitioning tracers, tracers of first type (Jin et al. 1995; Whitley 1997; Vulava et al. 2002). Perfluorides, such as perfluorodimethylbutane, perfluoromethylpentane and perfluoromethylhexane, are strongly NAPL partitioning and are gas tracers of the second type (Senum et al. 1992). Alkanes, such as methane and ethane, have been found to be water but not NAPL

partitioning, tracer type (3) (Deeds et al. 1999b). Halons such as bromochlorodifluoromethane, dibromodifluoromethane, and difluorotetrabromoethane, are also water partitioning but are more strongly NAPL partitioning, tracer type (4), see Chapter 2 of this work.

If an instantaneous pulse is placed into the inlet stream of a vessel, then the one dimensional, Cartesian, convection-dispersion equation describing transport the conservative tracer, tracer type (1) is (Levenspiel 1972):

$$\theta_g \frac{\partial C_g}{\partial t} = \theta_g D \frac{\partial^2 C_g}{\partial x^2} - u \frac{\partial C_g}{\partial x} \quad (1)$$

The dimensionless form of this equation is:

$$\frac{\partial C^*}{\partial T^*} = \left(\frac{D}{uL} \right) \frac{\partial^2 C^*}{\partial x^{*2}} - \frac{\partial C^*}{\partial x^*} \quad (2)$$

Please see the nomenclature section for variable definitions.

The first time moment of the curve is calculated by the following equation:

$$t^* = \frac{\int_0^{\infty} t C dt}{\int_0^{\infty} C dt} \quad (3)$$

If the curve is symmetrical, then the variance of the curve is the second moment of the curve relative to its mean can be described as sigmoidal (Levenspiel 1972):

$$\sigma^2 = \frac{\int_0^{\infty} (t - t^*)^2 C dt}{\int_0^{\infty} C dt} \quad (4)$$

The higher the level of dispersion for the flow through the vessel, the greater the variance of the curve. The Peclet Number, Pe , can be obtained from the mean and the variance of the curve:

$$\sigma^{*2} = \frac{\sigma^2}{t^{*2}} = 2 \left(\frac{D}{uL} \right) = \frac{2}{Pe} \quad (5)$$

The Pe number is the ratio of the product of the average fluid velocity and the nominal length of fluid travel divided by the effective dispersion coefficient of the solute in the media. Thus, the purpose of the first set of tracers, the nonsorbing tracers, is to determine

the velocity and flow path of the extracted vapor as it is affected by the heterogeneity of the vadose zone geology, as determined from the dimensionless variance of the tracer breakthrough curve. Levenspiel (1972, p. 275) reports that at high levels of dispersion the curve is no longer symmetrical. Assuming that the second moment is symmetrical results in an error of less than 5% for $Pe > 100$ and less than 0.5% for $Pe > 1000$.

If a gas tracer is NAPL partitioning, water partitioning and soil sorbing, then a mass balance for a representative volume in the unsaturated zone is:

$$\frac{\partial}{\partial t}(\theta_g C_g + \theta_n C_n + \theta_w C_w + \rho_b C_s) = D \frac{\partial^2 \theta_g C_g}{\partial x^2} - u \frac{\partial \theta_g C_g}{\partial x} \quad (6)$$

The partition coefficient, K_i , of a substance is the ratio of the concentration of the substance in one phase to the concentration of the substance in another. Each partition coefficient in equation (18) is defined in equation (11):

$$K_N = \frac{C_n}{C_g}; \quad K_H = \frac{C_g}{C_w}; \quad K_D = \frac{C_s}{C_w}; \quad (7)$$

Substituting the appropriate relationship for the respective concentrations, C_n , C_w , and C_s , leads to:

$$\left(1 + \frac{K_N \theta_n}{\theta_g} + \frac{\theta_w}{K_H \theta_g} + \frac{K_D \rho_b}{K_H \theta_g} \right) \frac{\partial C_g}{\partial t} = D \frac{\partial^2 C_g}{\partial x^2} - u \frac{\partial C_g}{\partial x} \quad (8)$$

Specifically, the dimensionless saturations (S_w , S_n and S_g) are the fractional volume of pore space occupied by the respective phase. By substituting the saturation values in

Equation (8), a retardation factor for a NAPL partitioning, water partitioning, and soil sorbing tracer moving with gaseous flow in the unsaturated zone can be defined (Brusseau et al. 2003a) :

$$R_i = \frac{t_p}{t_c} = 1 + \frac{K_{Ni}S_n}{S_g} + \frac{S_w}{K_{Hi}S_g} + \frac{K_{Di}\rho_b}{\theta K_{Hi}S_g} \quad (9)$$

This test was conducted at a site with a very low fraction of organic content, 0.00022. Therefore, the retardation of all of the tracers was negligible and the last term in Equation (9) is neglected for this work.

For a conservative tracer, such as helium, the retardation factor is equal to one. The perfluoride tracers have low soil sorption coefficients, high NAPL-air partition coefficient and high Henry's Law Constants (see Table 4.1), therefore the perfluorides' retardation factor are:

$$R_p = 1 + \frac{K_{NP}S_n}{S_g} \quad (10)$$

The alkanes' Henry's Law constants are high and the NAPL-air partition coefficient negligible (Deeds et al. 1999b). Therefore, the alkane retardation factors are:

$$R_A = 1 + \frac{S_w}{K_{HA}S_g} \quad (11)$$

The above analysis differs from Deeds et al. (1999b) who assume that there is negligible alkane partitioning into the water phase.

While the NAPL-air partition coefficient for the halons are significantly higher than their Henry's Law Constants, water partitioning can still be significant (see Chapter 2). The halons' retardation factors are:

$$R_H = 1 + \frac{S_w}{S_g K_{HH}} + \frac{K_{NH} S_n}{S_g} \quad (12)$$

The above analysis also differs from (Whitley et al. 1999) who assume that there is a negligible water phase for their porous media.

Materials and Methods

This study took place at the Tucson International Airport Superfund Site. Past practices at the site have resulted in volatile organic compound contamination of the subsurface. A soil vapor extraction pilot test and partitioning tracer test were performed at a site after several triple completion wells were drilled prior to the start-up of a full-scale remedial soil vapor extraction system. The locations of the test well and piezometers are presented in Figure 4.1, and the screen intervals for the middle and deep depths at the nested locations are presented in Table 4.2. Figure 4.2 illustrates the well completion details in a NE/SW direction, and Figure 4.3 denotes the NW/SE line of well completions with their

respective stratigraphies. Stratigraphic interpretation defines the first 3 to 5 meters below ground surface (bgs) at the site as fill, the next 6 to 12 m bgs as clay (USGS ML), and from 12 to 23 m bgs as sand (USGS SC). Core data for this formation, obtained from a sonically drilled well, have an average total porosity value, θ , of 0.43 ± 0.6 , bulk density, ρ_b , 1.37 ± 0.12 g/mL, and total organic carbon fraction, f_{oc} , of 0.0002 ± 0.0001 (Brusseau 1997).

The total volume of this clay formation for the area of influence for this SVE system was estimated to be approximately 50,000,000 L by interpolating the well logs by the Rockworks® software by an inverse distance interpolation scheme. The areal extent of this volume is shown on Figure 4.1. The formation of interest is a fairly continuous, fractured clay structure 21 m thick, from 23 to 44 m bgs.

The chemicals used in this study, acronyms, CAS numbers, and related chemical properties are presented in Table 4.1. The tracers selected for use have low toxicity, low background levels, low biodegradation or other transformation reactions, and low sorption to porous media.

Vapor effluent from the extraction well was pulled by a five-horsepower (EG&GE) blower, supplied by R.E. Wright (Allentown, PA). Discharge from the blower unit was routed through two 455-kg units of activated carbon (Carbtrol, Bridgeport, CT) connected

in series. The ambient and gas stream temperatures and relative humidities were measured via an Omega Model #RH30F (Stamford, CT) handheld temperature /humidity meter. The effluent volumetric flow rate was determined by a Kurz Minianemometer Series 490IS (Monterey, CA) pipe inner diameter. Vacua were measured via seven Dwyer magnehelic gauges (Vancouver, BC) gauges calibrated in the ranges of 0 to 0.1, 0 to 1, 0 to 5, 0 to 10 and 0 to 50, 0 to 100, and 0 to 500 inches water column (in H₂O) vacuum.

Gas samples were collected via a gas sampling pump (Tracer Research, Tucson, AZ) via 1-mL syringe (Terumo, Elkton, MD) and injected into field gas chromatographs via 10- μ L syringes (Hamilton Model 701, Reno, NV). Two field Hewlett Packard 5850 gas chromatographs (GCs) and Series II integrators were used to measure tracer gas concentrations were on-site to perform chemical analyses of the extracted gas. One GC was equipped with an electronic capture detector (ECD) to detect the perfluoride and halon tracers. The second GC was equipped with a flame ionization detector (FID) in order to measure methane, ethane and the background volatile organic compounds (VOCs). Helium was detected via a Veeco MS-50 Dual Port High Speed Leak Detector (Plainview, NY). Off-gas VOC concentrations were detected via an organic vapor analyzer (Hnu Model 102, Atlanta, GA) equipped with a photoionization detector (PID). Meteorological information was supplied by the Davis- Monthan Air Force Base. Groundwater levels were recorded via a Solinst water level meter (Georgetown, ON).

The SVE pilot test program was conducted using vacuum extraction wells and vacuum monitoring piezometers that were constructed for pilot testing and site-wide remediation activities. At each location, a nested well or nested piezometer was constructed with relatively short screened intervals at three discrete depths. Location P9 was selected as the extraction well due to it being centrally located amongst several piezometers and located within the contaminated soil zone. The middle screen depth from well P9 (P9M) was further selected as the depth to test, since it was reported to contain the greatest concentrations of volatile organic compounds (VOCs).

Throughout this study, vacuum was applied only to P9M. Vacua were measured at each of the three depths of the surroundings piezometers. This configuration produced radial flow into P9M. The formation produced low levels of effluent vapor (102 L/min +/- 54 L/min) at high vacuum (11.9 +/- 0.2 in Hg). The blower was operated at its highest sustainable vacuum and the vapor flow was not constant.

Tracers were inoculated into three wells surrounding P9M. VE305D was inoculated with He, PMCH and BCF and the response curve is Figure 5.4. VM301D was inoculated with M, PMCP and DTE and response is shown in Figure 5.5. VM302D was inoculated with E, PDMCB and DDM and the response is shown in Figure 5.6. The averages measured ambient background levels from Helium (5 µg/L), Methane (1.37 µg/L) and Ethane (0.29

µg/L) were subtracted from their reported values. The test was concluded before the levels of Methane, BCF, and DTE were reduced to baseline. Therefore their analysis included extending the curve by tail extrapolation until the tracer concentrations were equal to the detection limit (0.01 µg/L) (Deeds et al. 1999b).

The site was predominately contaminated with trichloroethene (TCE). Other volatile organic contaminants were 1,1-dichloroethene (1,1-DCE); freon-113 (F-113); and tetrachloroethene (PCE). The compounds 1,1,1-trichloroethane (TCA) was not detected in the extracted gas; PCE was detected only occasionally. High levels of 1,1-DCE, F-113 and TCE were consistently measured throughout the experiment. DCE coeluted with DTE and interfered with its detection. In addition to the field samples, gas canisters of the extracted gas were collected. Laboratory analyses of these canisters using different chromatographic columns were able to separate the DTE and DCE chromatographic peaks. Similarly, F-113 coeluted with DDM. The DDM tracer response was able to be distinguished from the F-113 by monitoring the level of F-113 and calculating an average value that was subtracted from the combined F-113 + DDM peak.

Results and Discussion

The piezometers (P6S and P9S) that were completed in the sand above the clay formation of interest exhibited very little vacuum throughout the project. Analysis of the vacuum response in the surrounding piezometers from the SVE pilot test were analyzed via the GASSOLVE program (Falta 1996) Table 4.3. The flow was assumed to be steady, open to the atmosphere, throughout the clay formation.

The average horizontal permeability from all field data was calculated to be approximately $0.75 \times 10^{-12} \text{ m}^2$; the vertical permeability was calculated to be $0.13 \times 10^{-12} \text{ m}^2$ giving an anisotropic ratio of 6. Freeze and Cherry (1979) report that clays typically have permeabilities in order of magnitude of 10^{-18} m^2 . A permeability of 10^{-12} m^2 is more typical of a sand formation. The vacuum response varied significantly throughout the field. No vacuum was measured at all three completions for P7 and P10, nor was any vacuum measured in any of the more shallow formations in wells completed above the clay formation.

The average travel time for the conservative tracers for the wells located 24 meters from the extraction well was 5000 min. The effective pore volume for this site was calculated to be $5000 \text{ min} * 100 \text{ L/min}$ or 500,000 L. Table 4.5 lists the respective effective dispersion coefficients, $D=uL/Pe$, calculated from the Peclet number, which in turn was calculated from the second moment ($Pe = 2/\delta^2$) for each compound.

The analyses of the three well tracer inoculations are listed in Tables 4.4 and 4.5. The mass recovery for each of the four classes of tracers were similar to each other. The perfluoride mass recoveries ranged from 23-48%, the alkane mass recoveries were 9.3-10%, and halon mass recoveries were 4.3 to 48 percent. The test had to be curtailed prior to the halon concentrations returning to baseline, so the halon mass recoveries were low. The BCF mass recovery was higher than the DDM and DTE because some of BCF mass recovered was from the earlier inoculation. The Helium mass recovery was very low, only 10%. Unlike the other gases, Helium is lighter than air, and may have preferentially risen out of the clay formation. The fact that the mass recovery was less than 50% for all tracers indicates that some tracer mass is diffusing out of the recovery path of the extraction well.

The true retardation factor could only be measured for the He-PMCH-DDM suite of tracers. The retardation factor for the other two suites were calculated by assuming that the S_n/S_g ratio for the perfluoride tracer is equal to that measured for the He-PMCH or

$$\frac{S_n}{S_g} = \frac{(R_p - 1)}{K_{Ni}} = \frac{R_{PMCH} - 1}{K_{PMCH}} = \frac{R_{PDMCB} - 1}{K_{PDMCB}} = \frac{R_{PMCP} - 1}{K_{PMCP}}$$

From these retardation factors, the water saturations for two alkane tracer suites, PDMCB-E-BCF and PMCP-M-DTE, were determined. The water saturation, S_w , for the He-PMCH-DDM suite of tracers could not be independently determined and so was

assumed to be the average of those determined via the alkane tracer suites. The water, NAPL, and gas saturation values are presented in Table 4.5. This study produced high S_w compared to other studies (Deeds et al. 1999a; Keller and Brusseau 2003; Mariner et al. 1999) and NAPL saturations are low. Keller and Brusseau cite accuracy difficulties with measuring water saturations at high water saturations.

A subsequent field-wide SVE project was conducted at this site from August 1996 to the present. In this project, vacuum is introduced to all of the ten triple completion wells. By multiplying the average NAPL saturation value (0.00071) times the total porous volume of the clay ($0.43 * 50,000,000$ L) that is expected to be influenced by the SVE system and assuming that the bulk of the contamination is TCE ($SG = 1.46$), the site wide estimated initial NAPL volume is 22,000 kg. This value is based on an assumption that the entire extent of the clay formation has porosities and NAPL saturations similar to those calculated from the PTT. This calculated initial NAPL value is in the same range but less than the total NAPL removed via the ongoing SVE project (28,600 kg) (Air Force, U.S. and R.S. Company 2004). The estimate obtained from the PTT test may be low because portions of the contaminant removal came from the upper formations at the TIA site that would not be detected by the PTT test. Volatile organic contaminants have been removed from the sand that is above the fractured clay formation.

The variance for the value for S_n were calculated by the following:

$$S_n = \frac{(R_p - 1)}{K_{NP}} S_g$$

$$\sigma^2(S_n) = \left(\frac{\partial S_n}{\partial (R_p - 1)} \right)^2 \sigma^2(R_p - 1) + \left(\frac{\partial S_n}{\partial (K_{NP})} \right)^2 \sigma^2(K_{NP}) + \left(\frac{\partial S_n}{\partial S_g} \right)^2 \sigma^2(S_g)$$

$$\left(\frac{\partial S_n}{\partial (R_p - 1)} \right) = \frac{S_g}{K_{NP}}$$

$$\left(\frac{\partial S_n}{\partial K_{NP}} \right) = - \frac{(R_p - 1)}{K_{NP}^2} S_g$$

$$\left(\frac{\partial S_n}{\partial S_g} \right) = \frac{R_p - 1}{K_{NP}}$$

The variances for the values of the NAPL-air partition coefficients for perfluoride tracers were presented in Chapter 2 of this dissertation. The average variance for the Henry's Law Constants for the halon tracers will be used for the variance for the alkane tracers, methane and ethane. The retardation factors for both the perfluoride and alkane partitioning tracers are experimentally determined by measuring tracer concentration

versus time. Since the Retardation Factor, R_i , is the ratio of the first moment of the partitioning tracer to the first moment of the nonpartitioning tracer, then the variance of R_i is equal to:

$$R_i = \frac{t_p}{t_c}$$

$$\sigma^2(R_i) = \left(\frac{\partial R_i}{\partial t_p} \right) \sigma^2(t_p) + \left(\frac{\partial R_i}{\partial t_c} \right) \sigma^2(t_c)$$

See Table 4.6 for the values of each of the terms in the above equations. For further discussion on quantifying the error in the analysis of partitioning tracer tests see Dwarakanath et al. (1999) and Payne (1999).

Conclusions

PTT technology is applicable in the vadose zone and can successfully determine NAPL, water and gas saturations. Reasonable NAPL volumes were calculated from this work even though it was conducted through a high water content, heterogeneous, fractured clay formation. Analysis of PTT in vadose zone requires an accounting of the tracer's partitioning from the gas phase into the NAPL and water phases.

Nomenclature

C	= concentration, $[ML^{-3}]$;
C^*	= dimensionless concentration, C/C_o , $[ML^{-3}/ML^{-3}]$;
C_o	= initial concentration, $[ML^3]$;
C_g	= tracer concentration in the gas phase, $[M/L^3]$;
C_n	= tracer concentration in the NAPL phase, $[M/L^3]$;
C_s	= sorbed mass fraction, [dimensionless];
C_w	= tracer concentration in the water phase, $[M/L^3]$;
D	= effective dispersion coefficient, $[L^2/t]$;
i	= partitioning tracer;
K_i	= partition coefficient, usually [-];
K_{Di}	= soil-water partition coefficient, $[L^3/M]$;
K_{Hi}	= gas-water partition coefficient, Henry's Law Constant, [-];
K_{Ni}	= NAPL-air partition coefficient, [-];
L	= characteristic length, $[L]$;
Pe	= Peclet Number, $Pe = uL/D$, [-];
R_i	= retardation factor, $R_i = t_p/t_c$, [-];
S_g	= gas phase saturation, [-];
S_n	= NAPL phase saturation, [-];
S_w	= water saturation, [-];
t	= time, $[t]$;

t^* = first time moment of tracer concentration breakthrough curve, mean travel time, [t];

T^* = dimensionless time, $T^* = t/t^* = tu/L$, [t/t];

u = superficial average fluid velocity, [L/t];

u_c = velocity of the conservative tracer, [L/t];

u_p = velocity of the partitioning tracer, [L/t];

x = spatial coordinate, [L];

x^* = dimensionless length, $x^* = (ux)/L$, [L/L];

θ = porosity of formation, [-];

σ = standard deviation, [same unit as parameter].

<p>Table 4.1 Physical and Chemical Information of Gas Tracers</p>						
Compound Name (Abbreviation)	CAS Number	Formula	Source (purity)	Soil-water Partition Coefficient ($K_D = 0.63 f_{oc} K_{ow}$) $f_{oc} = 0.00022$	Henry's Constant ($K_H = C_g/C_w$)	TCE-air Partition Coefficient ($K_N = C_n/C_g$)
Helium (He)	7440-59-7	He	Air Products (99%)	Not Applicable	Not Applicable	Not Applicable
Methane (M)	74-82-8	CH ₄	Scott Speciality Gases (97%)	2.49×10^{-3}	27 ¹	0 ²
Ethane (E)	74-84-0	C ₂ H ₆	Scott Speciality Gases (97%)	2.03×10^{-2}	20 ¹	0 ²
Perfluorodimethylcyclobutane (PDMCB)	2994-71-0	C ₆ F ₁₂	DuPont (97%)	2.13×10^{-5}	5,000 ³	22 ⁵
Perfluoromethylcyclopentane (PMCP)	180-22-7	C ₆ F ₁₂	Rhône-Poulenc (99%)	5.73×10^{-6}	2,000 ³	24 ⁵
Perfluoromethylcyclohexane (PMCH)	355-02-2	C ₇ F ₁₄	Rhône-Poulenc (99%)	2.28×10^{-5}	10,000 ³	53 ⁵
Bromochlorodifluoromethane (BCF)	353-59-3	BrClFC H	Great Lakes Chemical (99%)	4.66×10^{-1}	2 ⁴	420 ⁶
Dibromodifluoromethane (DDM)	75-61-6	CBr ₂ F ₂	Great Lakes Chemical (99%)	5.60×10^{-1}	2.9 ⁵	370 ⁵
Dibromotetrafluoroethane (DTE)	124-73-2	C ₂ Br ₂ F ₄	Great Lakes Chemical (99.9%)	6.29×10^{-2}	12 ⁵	470 ⁵

Table 4.1 Footnotes

1. (Mackay and Shiu 1981)
2. (Popovicova and Brusseau 1994)
3. In Chapter 3, I attempted to quantify the Henry's constant for these three perfluoride tracers. They were so water insoluble that reproducible numbers could not be obtained. The K_H presented is equal to Vapor Pressure /Water Solubility/(Universal Gas Constant * Absolute Temperature).
- 4.(Nelson et al. 1999a)
5. Chapter 2 of this work
6. Average of DDM and DTE partitioning values.

Table 4.2 Well Completion Information						
Well Name	Elevation (m) ¹	Depth to Top of Clay (m bgs) ²	Depth to Bottom of Clay ³ (m bgs)	Depth to Top of Screen (m bgs)	Depth to Bottom of Screen (m bgs)	Surface Radial Distance to Extraction Well (m)
P9 Extraction Well	791.55	25.9	36.6	S 12.5 M 28.5 D 35.5	S 15.5 M 33.0 D 49.0	0
VE305 Injection Well (He, PMCH, DDM into D)	791.01	24.4	34.1	S 22.0 M 26.2 D 30.6	S 24.9 M 29.2 D 33.6	14.4
VM301 Injection Well (PMCP, Methane, DTE into D)	790.93	22.3	34.6	S 21.9 M 26.2 D 30.6	S 24.9 M 29.2 D 33.5	24.1
VM302 Injection Well (PDMCB, Ethane, BCF into D)	790.64	20.6	34.0	S 21.7 M 26.2 D 30.6	S 24.7 M 29.1 D 33.5	24.1
VE303	790.91	20.3	34.0	S ⁴ 21.2 M 26.1 D 30.6	S 24.2 M 29.1 D 33.5	18.7

Table 4.2 Well Completion Information						
VE304	790.84	20.7	33.8	S 22.0 M 26.3 D 30.5	S 24.9 M 29.2 D 33.5	5.4
P6	791.10	18.9	42.7	S 13.4 M 28.1 D 34.7	S 18.0 M 32.7 D 46.9	9.7
P7	791.36	20.6	37.6	S 23.0 M 28.7 D 34.7	S 26.1 M 33.3 D 45.4	15.5
P8	791.43	19.5	42.7	S 12.7 M 28.5 D 35.1	S 15.8 M 33.1 D 48.8	8.7
P10	791.15	19.8	39.0	S 26.2 M 28.8 D 36.4	S 27.0 M 33.3 D 48.7	23.5

1. (m) = meters
2. (m bgs) = meters below ground surface
3. Or bottom of hole, as listed in **bold font**
4. All wells are triple completions. Shallow, Middle, Deep.

Table 4.3 TIA Site Permeability Calculations				
Well	Vacuum (in water)	Distance from P9M (meters)	k_r (m ²)	k_z (m ²)
VE305D	5.0	14	0.2×10^{-13}	0.1×10^{-13}
VM302D	2.3	24	0.8×10^{-14}	0.6×10^{-13}
VM301D	1.6	24	0.2×10^{-15}	0.8×10^{-13}

Table 4.4 Analysis of Moments - Tucson Airport Site Gas Partitioning Tracer Test									
Well	Mass Injected (g)	Mass Recovered (g)	Percentage of Injected Mass Recovered	First Moment (min)	Second Moment (min ²)	Dimensionless Second Moment	Peclet Number Pe	Linear Gas Velocity (cm/sec)	Effective Dispersion Coefficient (cm ² /sec)
VE305D									
He	10	1.0	10.	215	1.06×10^4	0.23	8.7	0.11	18.6
PMCH	50	11.	23.	300	3.14×10^4	0.35	5.7	0.08	20.3
DDM	10	0.43	4.3	420	3.94×10^4	2.2	0.9	0.0575	92.9
VM302D									
Non-reactive				5,500					
PDMCB	50	15.	30.	6,400	1.84×10^7	0.45	4.4	0.0063	3.40
Ethane	50	4.6	9.3	7,100	1.21×10^7	0.24	8.4	0.0057	1.63
BCF ¹	5	2.4	48.	24,000	3.94×10^8	0.70	2.9	0.0017	1.40
VM301D									
Non-reactive				4,400					
PMCP	50	24.	48.	5,200	9.24×10^6	0.34	5.9	0.0077	3.17
Methane	100	10.	10.	8,100	1.34×10^7	0.20	9.8	0.0050	1.22
DTE ¹	5	0.92	4.3	16,500	1.67×10^8	0.63	3.2	0.0024	1.83

Table 4.4 Footnote

1. The **first and second moments** for the Methane, BCF and DTE curves were calculated by extending the breakthrough curve via a semilog plot until the tracer concentrations were equal to the detection limit (0.01 $\mu\text{g/L}$).

Table 4.5 Saturation Calculations - Tucson Airport Site Gas Partitioning Tracer Test				
Well	Retardation Factor	Water Saturation	NAPL Saturation	Gas Saturation ¹
VE305D				
He	1.00	0.9055 ²	0.00071	0.0938
PMCH	1.40			
DDM	1.95			
VM302D				
Nonreactive	1.00	0.8535	0.0011	0.1454
PDMCB	1.17			
Ethane	1.29			
BCF	4.37			
VM301D				
Nonreactive	1.00	0.9575	0.00032	0.0422
PMCP	1.18			
Methane	1.84			
DTE	3.75			

1. The listed gas saturation, S_g , is equal to $1-S_w-S_n$.

2. Since there was no significant water partitioning tracer in this triplet, the average water saturation for the other two suites was assumed.

Table 4.6 Analysis of S_n Variance												
Tracer	$\frac{[\partial S_n]^2}{[\partial(R_p-1)]}$	$\sigma^2(R_p-1)$	Total (R_p-1) Variance	Percent of Total S_n Variance due to R_p	$\frac{[\partial S_n]^2}{[\partial K_{NP}]}$	$\sigma^2(K_{NP})^1$	Total K_{NP} Variance	Percent of Total S_n Variance due to K_{NP}	$\frac{[\partial S_n]^2}{[\partial S_g]}$	$\sigma^2(S_g)$	Total S_g Variance	Percent of Total S_n Variance due to S_g
PDMCB	4.4×10^{-5}	2.8×10^{-2}	1.2×10^{-6}	43%	1.2×10^{-7}	12	1.5×10^{-6}	52%	6.0×10^{-5}	2.7×10^{-3}	1.6×10^{-7}	5%
PMCP	3.1×10^{-6}	2.8×10^{-2}	8.7×10^{-8}	3%	9.8×10^{-8}	29	2.8×10^{-6}	92%	5.6×10^{-5}	2.7×10^{-3}	1.5×10^{-7}	5%
PMCH	3.1×10^{-6}	2.8×10^{-2}	8.8×10^{-8}	3%	2.0×10^{-8}	150	3.0×10^{-6}	92%	5.7×10^{-5}	2.7×10^{-3}	1.5×10^{-7}	5%

¹ The variance from the K_{NP} is presented in Chapter 2.

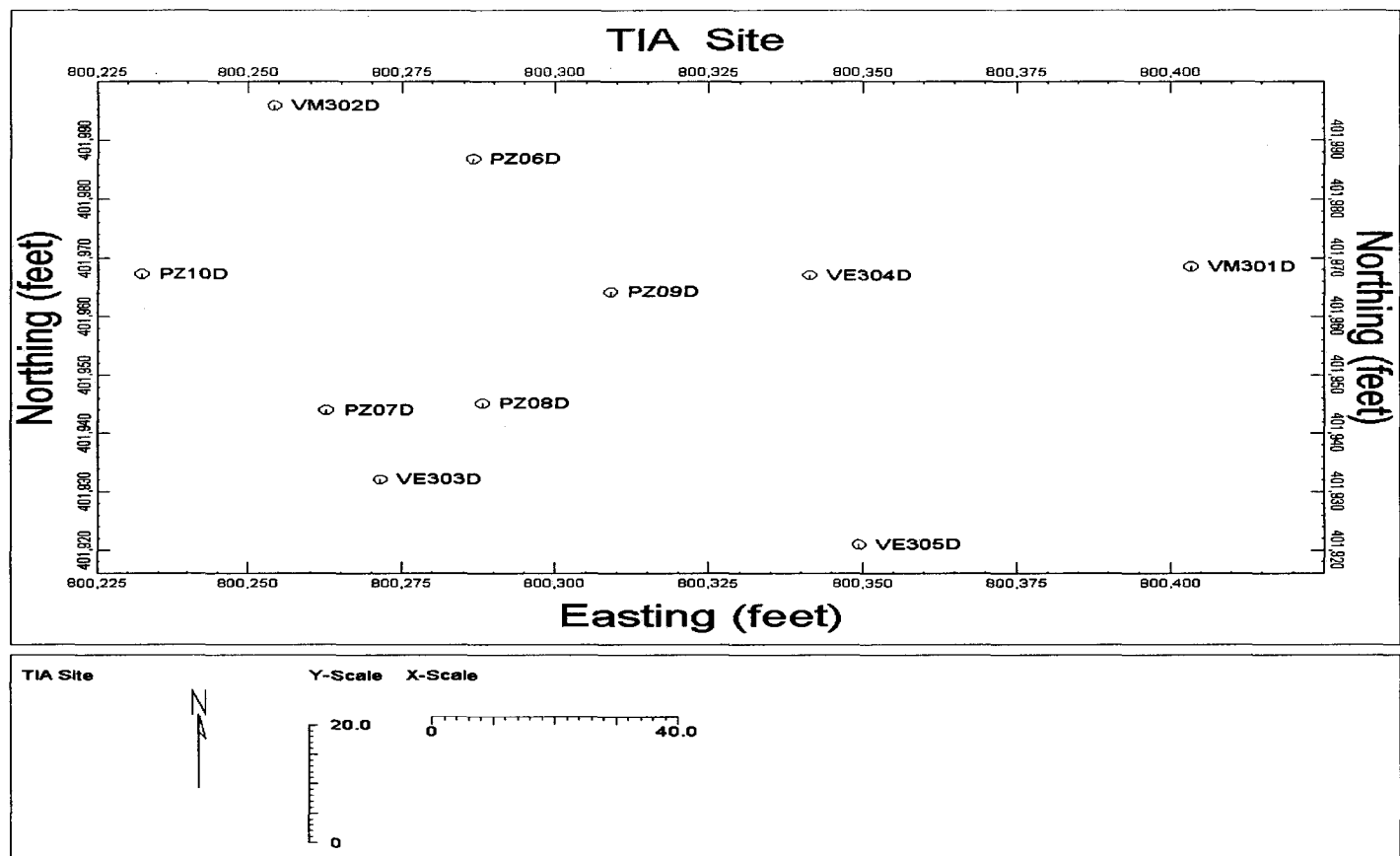


Figure 4.1 Tucson International Airport Site Map

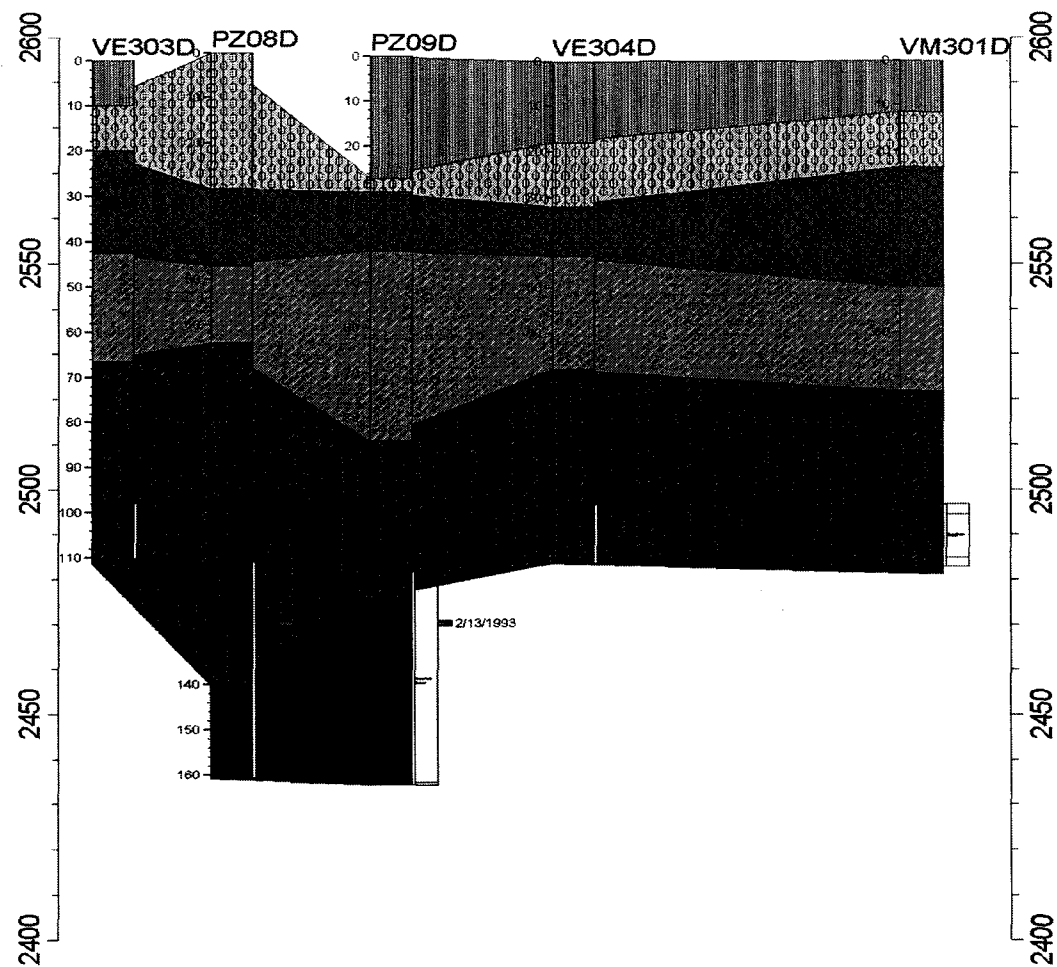


Figure 4.2 Illustration of the stratigraphy and well completion details in a NE-SW direction

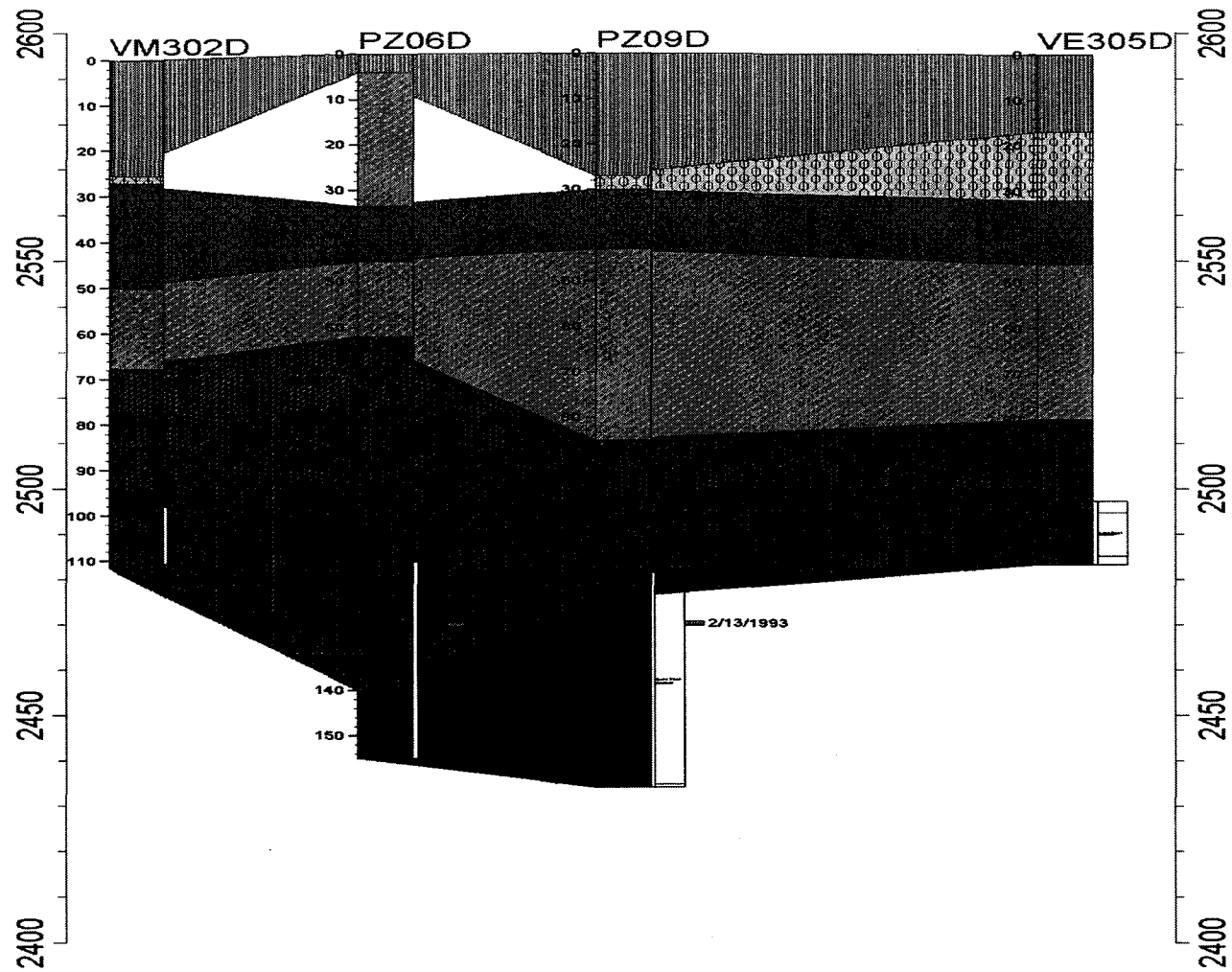


Figure 4.3 Illustration of the stratigraphy and well completion details in a NE-SE direction

VE305

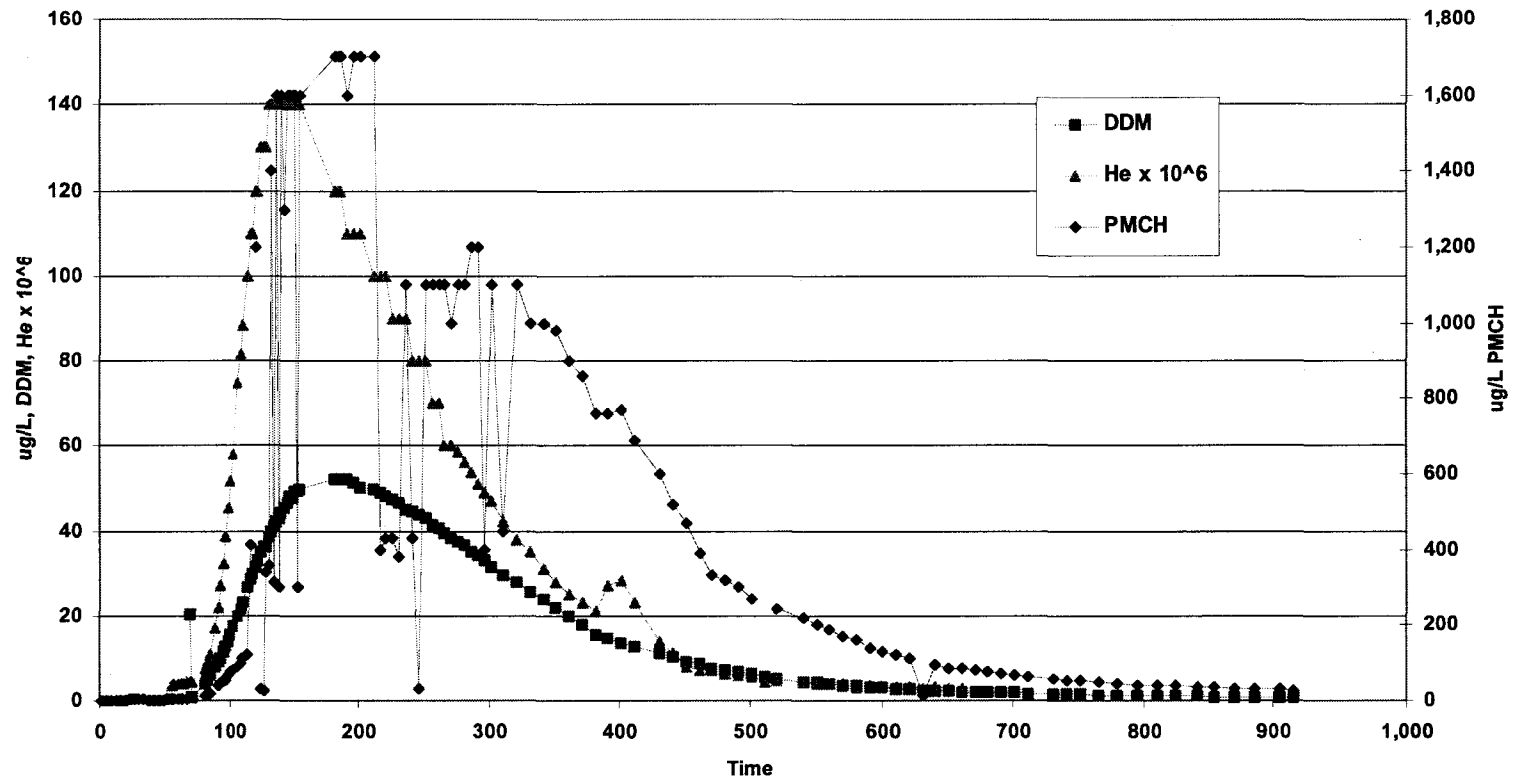


Figure 4.4 VE305D Tracer Concentration Breakthrough Curve versus Time

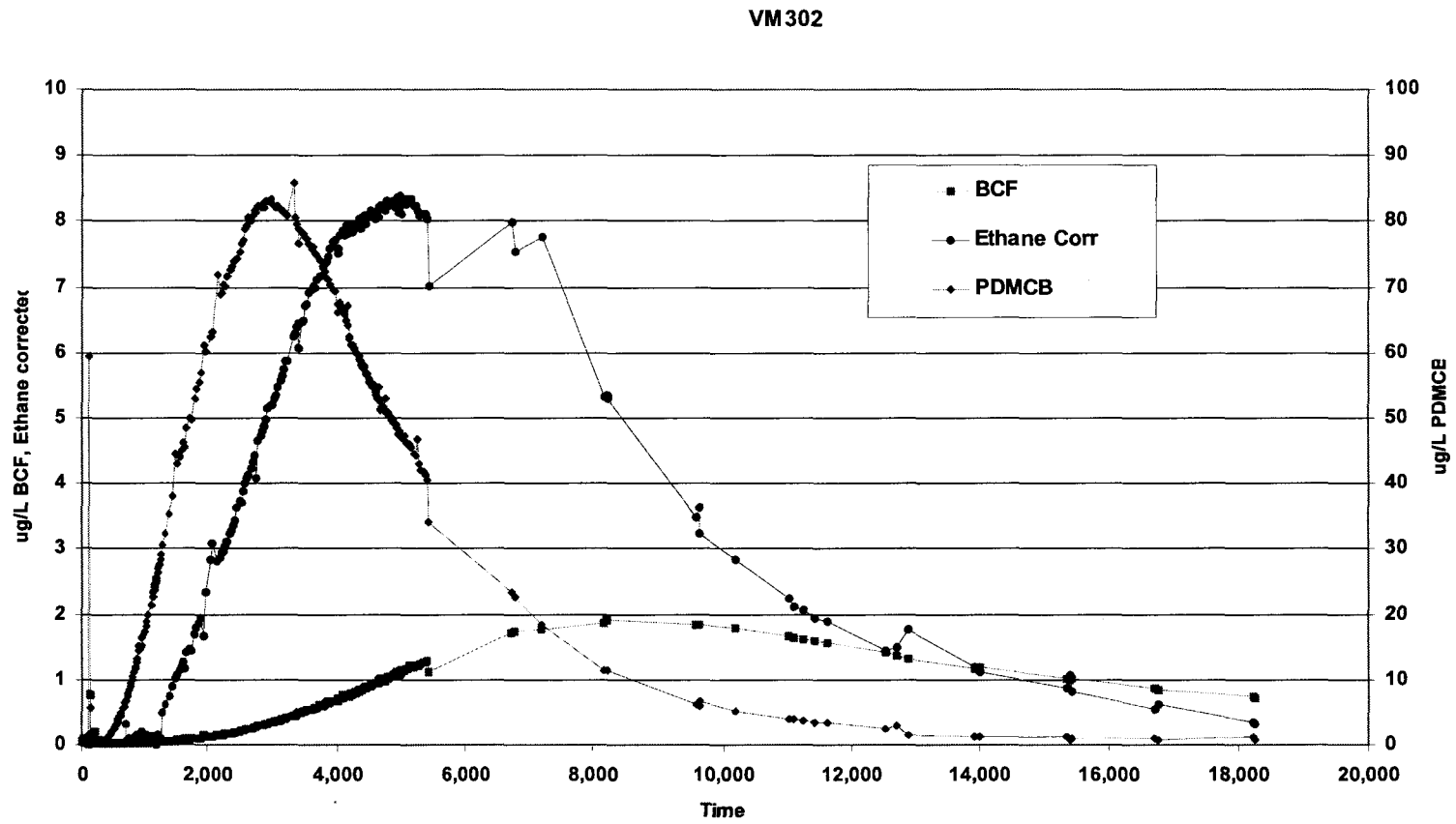


Figure 4.5 VM302D Tracer Concentration Breakthrough Curve versus Time

VM301

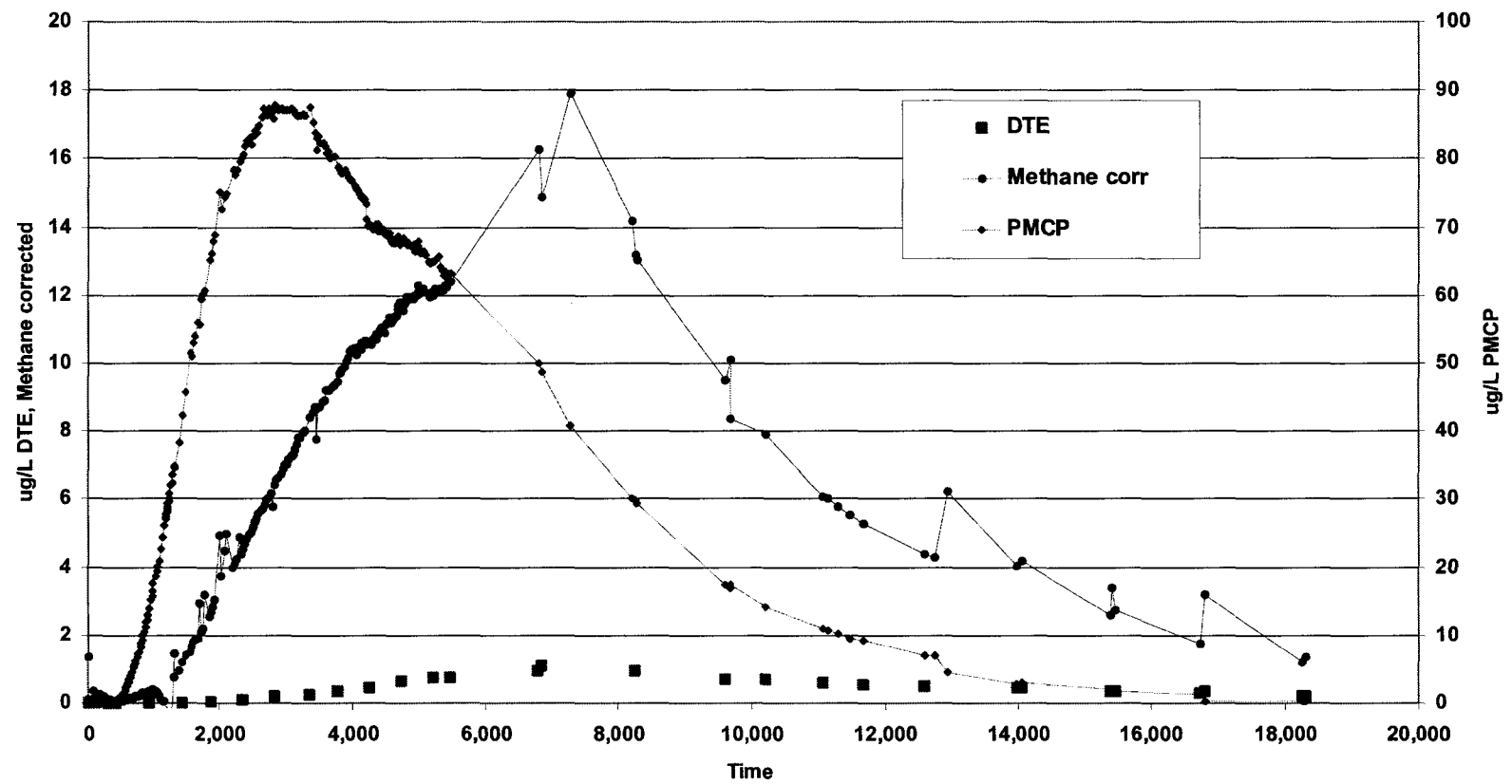


Figure 4.6 VM301D Tracer Concentration Breakthrough Curve versus Time

CHAPTER 5. USING SIMPLE SPREADSHEET MODELS TO ANALYZE GAS PHASE TRACER TESTS CONDUCTED IN FRACTURED MEDIA

Introduction

Fluid production through fractured formations is of interest to practitioners in many disciplines such as petroleum, hydrogeology, environmental, geothermal and nuclear. Modeling fracture flow has been well documented through the years and compiled into compendia. Most of the formation parameters used in modeling, whether for fracture or for porous media flow, have been determined from pressure and tracer tests. Pressure tests can determine formation permeability, fluid conductivity, well radius of effective flow, and interwell fluid communication. Tracer tests also can confirm interwell communication, as well as effective porosity and effective dispersion coefficients. Partitioning tracer tests can determine non aqueous phase, water, and gas saturations. Laboratory- and field-scale tracer tests have been successfully modeled numerous times.

Bear and coauthors (Bear et al. 1993) published an exhaustive text on fracture flow. Many workers on the Yucca Mountain Nuclear waste project have developed models; (Dobson et al. 2003; Hinds et al. 1999; Huang et al. 1999; Mukhopadhyay and Tsang 2002; Wu and Pruess 2000) are some of the more recent papers. Earlougher (1977) wrote the petroleum engineer's primer on reservoir pressure response analyses and devotes several sections on fracture flow. The fractured rock geothermal fields have been extensively studied and documented (cf. Hunt 1998; Khutorskoi et al. 2004; Bem et al.

2004; and Wood et al. 2004).

The early work relied on generating basic curves of response for various parameters, plotting dimensionless experimental data in the same scale and performing graphical curve fitting. Later work would see the automation of this process by using computer solving techniques (Horne 1995). The United States Salinity Laboratory has developed numerical codes for estimating transport parameters (Toride et al. 1995) from numerically integrating analytical models. Many models employ analytical solutions solved in Laplacian space and are then numerically inverted (cf. Becker and Charbeneau 2000). Numerical models are becoming increasingly complex. A recent study, developed by Bogdanov and coworkers (Bogdanov et al. 2003a, 2003b), relies on a three-dimensional, tetrahedral numerical model. Publically available numerical models such as TMVOC, UTCHEM, and MODFLOW SURFACT have dual porosity options for fracture flow. Wörman et al. (2003) developed a rigorous stochastic model for solute mass flows in fractured rock.

While the complexity and rigor of the work of Bogdanov et al. and Wörman et al. is impressive, not all projects and investigators are able to acquire the data necessary to completely utilize these models. This project follows a simpler approach. Bullivant and O'Sullivan (1989) compared radioactive tracer test results from the Wairakei Field to simulations produced with two porous, three double-porosity and three fracture-based

models. Akin (2001) developed an Excel® spreadsheet based on Bullivant and O'Sullivan's work, by using the Excel® spreadsheet tool Solver®, to minimize model residuals and determine transport parameters. Akin's spreadsheet can be obtained from the Computers and Geosciences webpage: www.iamg.org/.

This chapter is a continuation of Bullivant and O'Sullivan and Akin's work. Transport parameters have been estimated by matching tracer concentration data from a partitioning tracer test performed at a Tucson Arizona Superfund Site. This work differs from the earlier work in that it was a radially convergent gas-phase tracer test performed in the vadose zone. Most of the fracture tracer models developed to date, especially the analytical models, were developed for uniform aqueous flow in Cartesian coordinates.

Aqueous flow in porous media is assumed to follow Darcy's law (Fetter 1993). Baehr and Hult (1991) state that Darcy's law can be used to describe advective gas flow in most cases, except when the permeability is small and the applied vacuum is large. Falta (1996) and Joss and Baehr (1997) have successfully developed analytical solutions for radially convergent gas flow so that vacuum tests can be used to determine formation permeability. This work extends this concept to gas-phase partitioning tracer tests.

Experimental Method

In Chapter 4, it was reported on the phase saturations as determined from a gas phase

partitioning tracer test performed in a fractured clay formation at the Superfund Site in Tucson, AZ. The significant formation parameters are presented in Table 4.1. There were two different inoculations performed at this site. In the first inoculation, three different suites of tracers were inoculated into three wells located 5.4 to 9.7 m from a single extraction well. Well-defined tracer concentration breakthrough curves were not developed for two of these three initial inoculation wells because the peak concentration occurred earlier than anticipated. It was therefore decided to perform a second inoculation with the same three suites of tracers into wells located 14.5 to 24 m from the extraction well. The analysis of the second inoculation is presented in Chapter 4.

The determination of transport parameters via the analysis of the tracer breakthrough curves is presented in this chapter. The following analyses are based on the perfluoride, alkane, and halon tracer data from two wells, P8M and VM302D, from this experiment. These two wells were chosen because the tracers inoculated are the same and their measured retardation factors are similar: PDMCB ($R_f = 1.17$ for both wells), Ethane ($R_f = 1.24$ for P8M and $= 1.29$ for VM302D), and BCF ($R_f = 2.43$ for P8M and $= 4.37$ for VM302D). Curve-fitting was performed on tracer concentration versus time divided by the tracer's retardation factor. Well P8M was located 8.7 meters from the extraction well, P9M, while well VM302D was located 24.0 meters away.

The mass transport parameters, such as the ratio of transport by advection to that of

dispersion (Peclet Number), were developed from reactor transport theory. Himmelblau and Bischoff (1968), Levenspiel (1972), and others have discussed the theory of age distribution functions. Kreft and Zuber (1978) and Parker and van Genuchten (1978) show that this theory of age distribution functions applies only if the tracer is injected into a reactor and measured as it flows out of the reactor. The tracer concentration in the resident fluid is not the same as it is in fluid flux. Parker and van Genuchten show that both resident and fluid flux concentrations obey the advection-dispersion equation but do not transform identically. Solutions of the advection-dispersion equations for a semi-infinite system during steady flow subject to a first-type inlet boundary condition yield flux concentrations while those subject to the third-type yield volume average concentrations. Toride et al. (1995), among others, shows that the resident and flux-averaged concentration can be the same under specific initial and boundary conditions. Flux-averaged concentrations (C) will be presented in this work. Definitions of variables are presented in the Nomenclature section.

Model Methods

Porous, Uniform Flow, Cartesian One- and Two-Dimensional Model

Sauty (1980 and 1978) developed a solution for an instantaneous slug flowing through an uniform flow field in a homogeneous porous aquifer. He developed one- and two-dimensional solutions for Cartesian and radial coordinates. The Cartesian one-dimensional advection-dispersion transport equation of a pulse of tracer in a Cartesian coordinate system of uniform flow is:

$$\frac{\partial C}{\partial t} = -u \frac{\partial C}{\partial x} + D_L \frac{\partial^2 C}{\partial x^2}$$

The tracer concentration was flux-averaged from the extraction well, therefore the boundary conditions for this equation are:

$$C(0,t) - \frac{D_L}{u} \frac{\partial C(0,t)}{\partial x} = \frac{M}{Q} \delta(t)$$

The maximum concentration of the pulse, C_{max} , occurs at some time after injection, t_{max} , according to the following equations:

$$C_R(t_R, Pe) = \frac{J}{(t_R)^{1/2}} \text{Exp} \left[-\frac{Pe}{4t_R} (1 - t_R)^2 \right]$$

$$J = (t_{R \max})^{1/2} \exp \left[\frac{Pe}{4t_{R \max}} (1 - t_{R \max})^2 \right]$$

$$t_{R \max} = \left(1 + \frac{1}{Pe^2} \right)^{1/2} - \frac{1}{Pe}$$

where $t_R = t/t_c$, $C_R = C/C_{max}$. Sauty developed numerical solutions for radial flow via the a numerical code (Ramses). In his 1969 paper, Sauty presents semilog t_R versus C_R plots and instructs the reader to curve fit the plots. The Peclet number is determined by curve-fitting and then the longitudinal dispersivity and effective porosity are calculated by:

$$\alpha_L = \frac{R}{Pe}$$

$$\theta_e = \frac{Qt_c}{\pi R^2 h}$$

Sauty also developed the solution of a two-dimensional Cartesian and radial model:

$$C_R = \frac{J}{t_R} \exp \left[- \frac{Pe}{4t_R} (1 - t_R)^2 \right]$$

where

$$J = t_{R \max} \exp \left[\frac{Pe}{4t_{R \max}} (1 - t_{R \max})^2 \right]$$

$$t_{r \max} = \sqrt{1 + 4Pe^{-2}} - 2Pe^{-1}$$

Note that the Pe numbers are defined by the t_{Rm} and will be different for each model.

The unknown quantity for performing this calculation was the value for t_c , the transfer time by pure convection which is a function of the effective pore volume. Akin uses the Excel[®] Solver to optimize the Sauty Solution to experimental data by varying C_{max} , t_{max} , and t_c .

Single and Mulifracture Models

For the single and multifracture models, it is assumed that injection and extraction wells are connected by one or more highly permeable fractures surrounded by impermeable rock. Dispersion, due to the velocity profile across the fracture and molecular diffusion, moves tracer particles between streamlines by Taylor dispersion. (Horne and Rodriguez 1983) derived an expression for the Taylor dispersion coefficient, D_{Tr} (Taylor 1953).

$$D_{Tr} = \frac{2}{105} \left(u \frac{b}{2} \right)^2 \frac{1}{D_M}$$

Fossum and Horne (1982) determined effective fracture aperture for a fractured formation from the equation above.

The advection-dispersion equation for flow through the fractures is:

$$D_{Tr} \frac{\partial^2 C_f(x,t)}{\partial x^2} - \frac{Q}{A} \frac{\partial C_f(x,t)}{\partial x} = \frac{\partial C_f(x,t)}{\partial t}$$

The initial boundary condition is the pulse of tracer was introduced at the injection well:

$$C_f(0,t) - \frac{D_{Tr}}{u} \frac{\partial C_f(0,t)}{\partial x} = \frac{M}{Q} \delta(t)$$

$$C = J \frac{1}{\sqrt{t}} \frac{2t_m}{t} \exp \left\{ \frac{-Pe(t-t_m)^2}{4t_m t} \right\}$$

$$J = \left(\frac{M}{4Q} \right) \left(\frac{Pe}{\pi t_m} \right)^{1/2}$$

This work attempted to match the data for one and three fractures.

Fracture-matrix Model

It is assumed in this model that there is a large fracture with many smaller fractures in the

surrounding rock matrix. Tracer particles periodically enter and leave the microfracture network. Longitudinal dispersion across the velocity profile of the fluid flow in the fractures is ignored. The advection-dispersion equation for flow in the fracture:

$$-\frac{Q}{A} \frac{\partial C_f(x,t)}{\partial x} + 2 \frac{D_m}{a} \frac{\partial C_m(x,0,t)}{\partial z} = \frac{\partial C_f(x,t)}{\partial t}$$

Diffusion occurs within the matrix according to:

$$D_m \frac{\partial^2 C_m}{\partial z^2} = \theta_m \frac{\partial C_m}{\partial t}$$

The tracer concentration in the matrix is equal to the tracer concentration in the fracture at the boundary between the fracture and the matrix:

$$C_m(x, \frac{b}{2}, t) = C_f(x, t)$$

and the tracer is released into the fracture as a Dirac pulse:

$$C_f(0, t) = \frac{M}{Q} \delta(t)$$

The Jensen and Horne (1983) solution for the above is:

$$C = JU(t - t_c)^{-1/2} \exp\left\{\frac{-t_c}{w(t - t_c)}\right\}$$

$$J = \left(\frac{M}{Q}\right)\left(\frac{t_c}{\pi w}\right)^{1/2}$$

$$w = \frac{2}{3}\left(\frac{t_c}{t_{\max} - t_c}\right)$$

Double Porosity Models- Slabs and Cubes

One of the earliest models for fracture flow was developed by Warren and Root (1963). This model assumed that all advective flow occurred in the fracture and none in the matrix. The tracer could diffuse into the matrix and so the matrix could serve as a tracer mass source and sink. Several investigators developed solutions for different fracture/matrix geometries. There are several shapes for the fracture/matrix: parallel plates or slabs, cubes, or spheres. (Barker 1982) presented solutions to all three shapes; (Sudicky and Frind 1982), and (Maloszewski and Zuber 1985) used the double porosity slabic model for pressure modeling and (Bodvarsson and Tsang 1982) used the slabic solution for thermal modeling. (Lai et al. 1983) and (Bodvarsson and Tsang 1982) used the cubic and (Rasmuson and Neretnieks 1981) and (Rasmuson 1984) used the spherical for tracer tests. The double porosity model is used for publically available numerical

models such as TMVOC, UTCHEM and MODFLOW SURFACT

The double-porosity slabs model has parallel slabs of constant thickness, a , separated by fractures of constant separation, b . Tsang (1992) cautions that different authors define the fracture aperture as b or $2b$ and cautions readers to be vigilant when using the various models. Bullivant and O'Sullivan report that the fracture/block interface area per unit formation volume is $2/(b+a)$ and the fracture volume per unit formation volume is $b/(a+b)$. Therefore, the governing equation for tracer flow in the fractures is:

$$-\frac{Q}{A} \frac{\partial C_f(x,t)}{\partial x} - D_m \frac{2}{a+b} \frac{\partial C_m(x, \frac{b}{2}, t)}{\partial z} = \frac{a}{a+b} \frac{\partial C_f(x,t)}{\partial t}$$

The tracer concentration at the interface between the fracture and the matrix are equal:

$$C_m(x, \frac{b}{2}, t) = C_f(x, t)$$

Diffusion occurs within the matrix according to:

$$D_m \frac{\partial^2 C_m}{\partial z^2} = \theta_m \frac{\partial C_m}{\partial t}$$

No tracer flows across the slab center line because of symmetry:

$$\frac{\partial C_m(x,0,t)}{\partial z} = 0$$

With the determination of three variables: t_c , the time that the pulse would reach the extraction well if there were no dispersion:

$$t_c = \left(\frac{a}{a+b} \right) \left(\frac{RA}{Q} \right)$$

t_f the time for the slabs to fill up with tracer:

$$t_f = \left(\frac{ba}{D_m} \right)$$

and w , the ratio of transport along the length of the fracture to transport out of the fracture:

$$w = \left(\frac{Q}{RA} \right) \left(\frac{a^2}{D_m \theta_m} \right) \left(\frac{a+b}{a} \right)$$

the solution for the slabic double porosity model is:

$$C = J \exp \left\{ -t_c \left[2 \sqrt{\frac{p}{wt_c}} \tanh \left(\frac{t_f}{2} \sqrt{\frac{p}{wt_c}} \right) + p \right] \right\}$$

$$J = \frac{M}{Q}$$

$$\frac{\theta_f}{\theta_m} = (1 - \theta_f) \frac{wt_b}{t_f} \approx \frac{wt_b}{t_f}$$

The cubic double-porosity solution is very similar to the slabic solution, but the cubic solution allows for advective flow in the vertical direction. Tracer movement into the matrix is modeled by diffusion perpendicular to the nearest face. The area of the surface at a distance $b/2 - z$ is equal to z^2 . The fracture/block interface area per unit volume is $6b/(a+b)^3$ and $\theta_f = 1 - b^3/(a+b)^3$. The governing equation is:

$$-\frac{Q}{A} \frac{\partial C_f(x,t)}{\partial x} - D_m \frac{6b^2}{(a+b)^3} \frac{\partial C_m(x, \frac{b}{2}, t)}{\partial z} = \frac{(a+b)^3 - b^3}{(a+b)^3} \frac{\partial C_f(x,t)}{\partial t}$$

The advection-dispersion equation of flow in the matrix is:

$$D_m \left(\frac{\partial^2 C_m(x, z, t)}{\partial z^2} \right) + \frac{2}{z} \frac{\partial C_m(x, z, t)}{\partial z} = \theta_m \frac{\partial C_m(x, z, t)}{\partial t}$$

The other boundary conditions are the same for the slabic solution: the tracer concentrations are equal at the fracture-matrix interface and symmetry holds.

Akin presented Barker's (1982) double-porosity cubic solution:

$$C = J \exp \left\{ -t_c \left[2 \sqrt{\frac{p}{wt_c}} \coth \left(\frac{t_c}{2} \sqrt{\frac{p}{wt_c}} \right) - \frac{4}{t_f} + p \right] \right\}$$

$$J = \frac{M}{Q}$$

and

$$t_c = \left(\frac{(a+b)^3 - b^3}{(a+b)^3} \right) \left(\frac{RA}{Q} \right)$$

$$t_f = \left(\frac{1}{D_m} \right) \left(\frac{(a+b)^3 - b^3}{3b} \right)$$

$$w = \left(\frac{Q}{RA} \right) \left(\frac{1}{D_m \theta_m} \right) \left(\frac{(a+b)^3}{(a+b)^3 - b^3} \right) \left(\frac{(a+b)^3 - b^3}{3b^2} \right)$$

Akin's spreadsheet solution solved for a best fit of t_e , t_p , and w .

Double Porosity - Pseudo Steady State or First Order Mass Transfer

Bullivant and O'Sullivan and Akin also discuss another double porosity model, which they call the pseudo steady state model. It is based on Warren and Root (1963) and Coats and Smith (1964) dead end pore model. Coats and Smith's developed a first-order mass transfer exchange relation for solute exchange between immobile fluid zones and the longitudinal flowing fluid as opposed to modeling based on Fickian diffusion. The advection-dispersion equation for fracture flow:

$$-\frac{Q}{A} \frac{\partial C_f}{\partial x} - \beta (C_f - C_m) = \theta_f \frac{\partial C_f}{\partial t}$$

Advective fluid flow through the matrix is assumed to be negligible and the conservation of mass equation for the matrix is:

$$\beta(C_f - C_m) = \theta_m \frac{\partial C_m}{\partial t}$$

The pulse of the tracer at the release well is:

$$C_f(0, t) = \frac{M}{Q} \delta(t)$$

and the tracer concentrations at the fracture matrix interface are equal. van Swaaij et al. (1969) and Villiermaux and van Swaaij (1969) developed the analytical solution for this problem and (Raven et al. 1988) numerically integrated the Villiermaux and Van Swaaij solution. The Akins spreadsheet solution is:

$$C = J \exp\{-\beta_m t\} U(t - t_c)^{1/2} * I_1 \left\{ 2(t_c \beta_f \beta_m (t - t_c))^{1/2} \right\}.$$

$$J = \left(\frac{M}{Q} \right) (t_c \beta_f \beta_m)^{1/2} \exp\{t_c (\beta_m - \beta_f)\}$$

$$\frac{\phi_f}{\phi_m} = \frac{\beta_m}{\beta_f}$$

The spreadsheet solves for best fit of t_c , β_f and β_m . The pseudo-steady state double-porosity solutions matched the experimental results consistently better than the slabic or cubic solutions.

Results and Discussion

Presented in Tables 5.3-5.8 and Figures 5.1-5.6 are the concentration breakthrough curves and modeled results for the two suites of tracers. All of the models could be reasonably fitted to the data. The two homogeneous physical domain (Sauty's 1-D and 2-D) models produced results very similar to each other. The homogenous models matched the VM304D BTCs better than the P8M breakthrough curves. The P8M BTC exhibited flow more consistent with fracture flow, as P8M was located closer to the extraction well than VM302D (8.7 versus 24.0 m). The fracture network behaved more like an equivalent porous medium than a fractured one for VM302D. Both of the porous media models underpredicted the early arrival times for the tracer and matched the later times, or the tails more closely.

The single fracture and the multifracture curve fits were very similar to each other for VM302D but the multifracture model was able to fit the P8M data more closely. These two fracture models underpredicted the tails. The fracture-matrix models consistently underpredicted the first arrival data while grossly over predicting the tails, as did the double porosity slabic and cubic models. The fracture-matrix model matched these data

the least well. Only the double-porosity pseudo steady state models under predicted the tails.

Conclusions

The obvious chief advantage of the simple models discussed above is that they are easy to implement. Different models gave different insight into different formation parameters.

The homogeneous models give the field wide averages for effective porosity and the effective dispersion coefficient which can be used for porous media modeling. The porous models can adequately predict field-wide mean arrival times but on the fracture models could be used to predict early first arrival times. Therefore, there are reasons to use both porous and fracture models.

Nomenclature

a = length of block side, [L]

A = total of all of the formation's stream tube cross section, [L²]

b = total aperture of fracture, [L]

C = flux-averaged concentration, [ML⁻³]

C_f = tracer concentration in fracture, [ML⁻³]

C_m = tracer concentration in matrix, [ML⁻³]

C_{\max} = maximum concentration of tracer pulse, [ML⁻³]

C_R = dimensionless concentration, C/C_{\max} , [-]

D_L = longitudinal dispersion coefficient, [L²T⁻¹]

D_M = molecular diffusion coefficient, [L²T⁻¹]

D_m = matrix diffusion coefficient, [L²T⁻¹]

D_{Tr} = Taylor dispersion coefficient, [L²T⁻¹]

h = formation thickness, [L]

I_1 = modified Bessel function of order one.

J = Model Parameter, definition and dimension are specific to model used

M_0 = mass of tracer initially injected, [M]

M = mass of tracer initially injected per unit area of formation section for one-dimensional model, [ML⁻²]

m = mass of tracer initially injected per unit thickness of formation section for two-dimensional model, [ML⁻¹]

N = dimensionless mass exchange constant, $= \kappa t_{\max}$, [-]

p = Laplace transform variable, $[T^{-1}]$

Pe = Peclet Number, [-]

Pe uniform flow $= (uR)/D = X/\alpha$,

Pe radial flow $= (u(R)*R)/D = R/\alpha$

q = darcy velocity, $[LT^{-1}]$

Q = flow rate from central well for radial flow, $[L^3T^{-1}]$, $Q > 0$ for injection, $Q < 0$ for production, $Q = -100$ L/min for this field test or $100,000$ cm³/min

r = distance to central well axis for radial flow, $[L]$

r_R = dimensionless distance to central well axis for radial flow, r/α , [-]

R = distance between extraction well and the injection well for radial flow, $[L]$

\mathbf{u} = effective velocity (mean pore velocity) vector, $[LT^{-1}]$

U = Heaviside step distribution

V = Darcy velocity, $[LT^{-1}]$

t = time, $[T]$

t_c = transfer time by pure convection or the time that the pulse would reach the observation well if there is no diffusion $[T]$

in uniform flow, equal to X/u

in radial flow, equal to $\omega \pi r^2 h / |Q|$

t_f = time for tracer to completely diffuse into matrix, $[T]$

t_m = mean residence time, as determined by first moment analysis, $[T]$

t_{\max} = time at which maximum concentration, C_{\max} , occurred, T

t_R = dimensionless time, t/t_m , [-]

w = ratio of transport along the fracture to transport out of the fracture, [-]

x = lateral component of distance from injection well to extraction well, [L]

x_R = dimensionless distance, x/R , [-]

z = vertical component of distance, [L]

α = dispersivity, [L]

α_L = longitudinal dispersivity, [L]

α_T = transversal dispersivity, [L]

β = rate of tracer interchange per unit of formation volume, [T⁻¹]

β_f = rate of tracer interchange per unit of fracture volume, [T⁻¹]

β_m = rate of tracer interchange per unit of matrix volume, [T⁻¹]

$\delta(t)$ = Dirac function, [T⁻¹]

θ = total porosity of formation, [-]

θ_f = fracture porosity of formation, [-]

θ_m = matrix porosity of formation, [-]

θ_e = effective porosity, [-]

Table 5.1
Formation Details

Symbol	Definition	Unit	Value
Q	Volumetric Flow rate	cm ³ /min	100,000
R	Linear Distance from Injection Well to Extraction Well	cm	870 cm (P8M) 2400 cm (VM302D)
θ	Total Porosity from Core Data	[-]	0.43

Table 5.2 Model Details			
	Solution	Characteristic Dimensionless Number Pe or w ¹	Parameters that are Adjusted for Curve- Fitting
Sauty 1-D	$C_R(t_R, Pe) = \frac{J}{(t_R)^{\frac{1}{2}}} \text{Exp} \left[-\frac{Pe}{4t_R} (1 - t_R)^2 \right]$ $J = (t_{R \max})^{1/2} \text{Exp} \left[\frac{Pe}{4t_{R \max}} (1 - t_{R \max})^2 \right]$	$Pe = \frac{2t_{R \max}}{1 - t_{R \max}}$	$t_{R \max} = t/t_m = \text{reduced time at } C_{\max}$ $t_c = \text{time for transport by convection only}$ $C_{\max} = \text{maximum concentration}$
Sauty 2-D	$C_R(t_R, Pe) = \frac{J}{t_R} \text{Exp} \left[-\frac{Pe(1 - t_R)^2}{4t_R} \right]$ $J = t_{R \max} \text{Exp} \left[\frac{Pe}{4t_{R \max}} (1 - t_{R \max})^2 \right]$	$Pe = \frac{4t_{R \max}}{1 - t_{R \max}^2}$	$t_{R \max} = t/t_m = \text{reduced time at } C_{\max}$ $t_c = \text{time for transport by convection only}$ $C_{\max} = \text{maximum concentration}$

Table 5.2 Model Details			
Single Fracture	$C(t) = \frac{J}{\sqrt{t}} \frac{2t_m}{t} \text{Exp} \left[-\frac{w}{4} \frac{(t - t_m)^2}{t_m t} \right]$ $J = \left(\frac{M}{4Q} \right) \left(\frac{Pe}{\pi t_m} \right)$	$w = \frac{(QR)}{D_{Tr} A}$	<p>J = model parameter t_m = first time moment of concentration breakthrough curve w = ratio of tracer transport by advection to tracer transport by diffusion</p>
Multifracture (Same as single fracture but flow is proportionately divided into two or more fractures)	$C(t) = \frac{J}{\sqrt{t}} \frac{2t_m}{t} \text{Exp} \left[-\frac{w}{4} \frac{(t - t_m)^2}{t_m t} \right]$ $J = \left(\frac{M}{4Q} \right) \left(\frac{Pe}{\pi t_m} \right)$	$w = \frac{(QR)}{D_{Tr} A}$	<p>J = model parameter t_m = first time moment of concentration breakthrough curve w = ratio of tracer transport by advection to tracer transport by diffusion</p>
Fracture-Matrix	$C(t) = JU(t - t_c) \frac{1}{(t - t_c)^{3/2}} \text{Exp} \left[-\frac{t_c}{w(t - t_c)} \right]$ $J = \left(\frac{M}{Q} \right) \left(\frac{t_c}{\pi w} \right)^{1/2}$	$w = \frac{Q}{RA} \left(\frac{a^2}{D_m \theta_m} \right)$	<p>J = model parameter t_c = time for transport by convection only w = ratio of tracer transport along fracture to tracer transport out of fracture</p>

Table 5.2 Model Details			
Double Porosity First Order Mass Transfer	$C(t) = J \text{Exp}[-\beta_m t] U(t - t_c) \frac{1}{(t - t_c)^{1/2}}$ $\bullet I_1 \left[2(t_b \beta_f \beta_m (t - t_c))^2 \right]$ $J = \left(\frac{M}{Q} \right) (t_c \beta_f \beta_m)^{1/2} \text{Exp} \left[t_c (\beta_m - \beta_f) \right]$	$w = 2$ $\bullet \left[t_c \beta_f \beta_m (t_{\max} - t_c) \right]^{1/2}$	<p>J = model parameter t_c = time for transport by convection only β_m = rate of tracer exchange per unit matrix volume β_f = rate of tracer exchange per unit fracture volume</p>
Double Porosity Slabs	$\bar{C}(p) = J$ $\bullet \text{Exp} \left\{ -t_c \left[2 \left(\frac{p}{wt_c} \right)^{1/2} \tanh \left[\frac{t_f}{2} \left(\frac{p}{wt_c} \right)^{1/2} \right] + p \right] \right\}$ $J = \frac{M}{Q}$	$w = \left(\frac{Q}{RA} \right) \left(\frac{a^2}{D_m \theta_m} \right) \left(\frac{a+b}{a} \right)$	<p>J = model parameter t_c = time for transport by convection only t_f = time for slabs to fill w = ratio of tracer transport along fracture to tracer transport out of fracture</p>

Table 5.2 Model Details			
Double Porosity Cubes	$\bar{C}(p) = J$ $\bullet \text{Exp} \left\{ -t_c \left[2 \left(\frac{p}{wt_c} \right)^{1/2} \coth \left[\frac{t_f}{2} \left(\frac{p}{wt_c} \right)^{1/2} \right] - \frac{4}{t_f} + p \right] \right\}$ $J = \frac{M}{Q}$	$w = \frac{Q}{RA} \frac{1}{D_m \theta_m} \left(\frac{(a+b)^3}{(a+b)^3 - a^3} \right)$ $\bullet \left(\frac{(a+b)^3 - a^3}{3a^2} \right)$	<p>J = model parameter t_c = time for transport by convection only t_f = time for slabs to fill w = ratio of tracer transport along fracture to tracer transport out of fracture</p>

- 1 Pe = Peclet Number = uR/D or w = ratio of transport along the fracture to transport out of the fracture
- 2 t_c = transfer time by pure convection or the time that the pulse w would reach the observation well if there is no diffusion
 t_m = mean residence time, as determined by first moment analysis
- 3 D = effective dispersion coefficient = uR/Pe or D_{Tr} = Taylor dispersion coefficient

Table 5.3 Comparison of All Models for PDMCB Inoculated into P8M						
	Sum of Square Residuals ($\mu\text{g/L}$) ²	Characteristic Dimensionless Number Pe or w^1	Characteristic Time ² (min)	Effective Dispersion Coefficient (cm^2/sec) ³	Average Radial Velocity (cm/min)	Fraction of flow per fracture
Method of Moments		1.1 (Pe)	490 (t_m)	190	4.9	1.0
Sauty 1-D	25,766	1.1 (Pe)	170 (t_m)	68.	5.2	1.0
Sauty 2-D	23,637	0.74 (Pe)	360 (t_m)	48.	2.4	1.0
Single Fracture	26,974	0.027 (w)	220,000 (t_m)	1600	0.0040	1.0
Multifracture (model assumed three fractures)	500	3800 (w_1) 36 (w_2) 5.4 (w_3)	350 (t_{m1}) 90. (t_{m2}) 600 (t_{m3})	0.58 240 230	2.5 10. 1.4	0.89 0.09 0.02
Fracture-Matrix	27,109	0.0010 (w)	0.10 (t_c)			1.00
Double Porosity First Order Mass Transfer	20,645	0.0025 (w)	14 (t_c)			1.0
Double Porosity Slabs	12,470	0.40 (w)	59 (t_c)			1.0
Double Porosity Cubes	12,478	0.40 (w)	59 (t_c)			1.0

- 1 Pe = Peclet Number = uR/D or w = ratio of transport along the fracture to transport out of the fracture
- 2 t_c = transfer time by pure convection or the time that the pulse would reach the observation well is there is no diffusion
 t_m = mean residence time, as determined by first moment analysis
- 3 D = effective dispersion coefficient = uR/Pe or D_{Tr} = Taylor dispersion coefficient

Table 5.4 Comparison of All Models for PDMCB Inoculated into VM302D						
	Sum of Square Residuals ($\mu\text{g/L}$) ²	Characteristic Dimensionless Number Pe or w^1	Characteristic Time ² (min)	Effective Dispersion Coefficient (cm^2/sec) ³	Average Radial Velocity (cm/min)	Fraction of flow per fracture
Method of Moments		4.4 (Pe)	6400 (t_m)	3.4 (D)	0.38	1.
Sauty 1-D	1,836	6.1 (Pe)	3300 (t_c)	4.7 (D)	0.72	1.
Sauty 2-D	2,119	5.9 (Pe)	3900 (t_c)	4.2 (D)	0.62	1.
Single Fracture	2,426	0.04 (w)	4700 (t_m)	3.7 (D)	0.51	1.
Multifracture (model assumed three fractures)	2,425	50 (w_1) 23 (w_2) 5.55 (w_3)	95 (t_{m1}) 180 (t_{m2}) 4700 (t_{m3})	20 (D_{Tr}) 23 (D_{Tr}) 3.7 (D_{Tr})	25 13 0.51	0.3 0.3 0.4
Fracture-Matrix	10,126	0.16 (w)	480 (t_c)			1.
Double Porosity First Order Mass Transfer	1,138	0.0023 (w)	820 (t_c)			1.
Double Porosity Slabs	25,434	0.64 (w)	410 (t_c)			1.
Double Porosity Cubes	25,434	0.52 (w)	415 (t_c)			1.

- 1 Pe = Peclet Number = uR/D or w = ratio of transport along the fracture to transport out of the fracture
- 2 t_c = transfer time by pure convection or the time that the pulse w would reach the observation well if there is no diffusion
 t_m = mean residence time, as determined by first moment analysis
- 3 D = effective dispersion coefficient = uR/Pe or D_{Tr} = Taylor dispersion coefficient

<p style="text-align: center;">Table 5.5 Comparison of All Models for Ethane Inoculated into PM8 (The Breakthrough Curve for Ethane was corrected for Background Levels)</p>						
	Sum of Square Residuals ($\mu\text{g/L}$) ²	Characteristic Dimensionless Number ¹ Pe or w	Characteristic Time ² (min)	Effective Dispersion Coefficient ³ (cm^2/sec)	Average Radial Velocity (cm/min)	Fraction of flow per fracture
Method of Moments		2.8 (Pe)	520 (t_m)	65. (D)	4.6	1.
Sauty 1-D	13,172	2.3 (Pe)	250 (t_c)	1300 (D)	3.5	1.
Sauty 2-D	13,789	2.1 (Pe)	380 (t_c)	960 (D)	2.3	1.
Single Fracture	14,730	0.0012(w)	310,000 (t_m)	730 (D)	0.0028	1.
Multifracture (model assumed three fractures)	7,628	12,000 (w_1) 140 (w_2) 4.4 (w_3)	300 (t_{m1}) 49. (t_{m2}) 430 (t_{m3})	0.22 (D_{Tr}) 110 (D_{Tr}) 730 (D_{Tr})	2.9 18. 2.0	0.07 0.79 0.13
Fracture-Matrix	14,943	0.0010 (w)	0.22 (t_c)			1.
Double Porosity First Order Mass Transfer	11,839	0.010 (w)	67. (t_c)			1.
Double Porosity Slabs	5,852	0.97 (w)	110 (t_c)			1.
Double Porosity Cubes	5,869	0.98 (w)	110 (t_c)			1.

- 1 Pe = Peclet Number = uR/D or w = ratio of transport along the fracture to transport out of the fracture
- 2 t_c = transfer time by pure convection or the time that the pulse would reach the observation well is there is no diffusion
 t_m = mean residence time, as determined by first moment analysis
- 3 D = effective dispersion coefficient = uR/Pe or D_{Tr} = Taylor dispersion coefficient

<p style="text-align: center;">Table 5.6 Comparison of All Models for Ethane Inoculated into VM302D (The Breakthrough Curve for Ethane was corrected for Background Levels)</p>						
	Sum of Square Residuals ($\mu\text{g/L}$) ²	Characteristic Dimensionless Number ¹ Pe or w	Characteristic Time ² (min)	Effective Dispersion Coefficient ³ (cm^2/sec)	Average Radial Velocity (cm/min)	Fraction of flow per fracture
Method of Moments		8.4 (Pe)	7100 (t_m)	1.6 (D)	0.34	1.
Sauty 1-D	15	4.9 (Pe)	5000 (t_c)	235 (D)	0.48	1.
Sauty 2-D	17	6.3 (Pe)	5100 (t_c)	180 (D)	0.47	1.
Single Fracture	20	0.0063 (w)	830 (t_m)	125 (D)	0.31	1.
Multifracture (model assumed three fractures)	8	0.06 (w_1) 12. (w_2) 8.6 (w_3)	330 (t_{m1}) 2500 (t_{m2}) 5800 (t_{m3})	290,000 (D_{Tr}) 190 (D_{Tr}) 115 (D_{Tr})	7.27 0.97 0.40	0.07 0.86 0.07
Fracture-Matrix	137	0.22 (w)	830 (t_c)			1.
Double Porosity First Order Mass Transfer	13	0.0016 (w)	970 (t_c)			1.
Double Porosity Slabs	9	0.13 (w)	415 (t_c)			1.
Double Porosity Cubes	13	0.40 (w)	1200 (t_c)			1.

1 Pe = Peclet Number = uR/D or w = ratio of transport along the fracture to transport out of the fracture

2 t_c = transfer time by pure convection or the time that the pulse would reach the observation well if there is no diffusion
 t_m = mean residence time, as determined by first moment analysis

3 D = effective dispersion coefficient = uR/Pe or D_{Tr} = Taylor dispersion coefficient

Table 5.7 Comparison of All Models for BCF inoculated into PM8						
	Sum of Square Residuals ($\mu\text{g/L}$) ²	Characteristic Dimensionless Number ¹ Pe or w	Characteristic Time ² (min)	Effective Dispersion Coefficient ³ (cm^2/sec)	Average Radial Velocity (cm/min)	Fraction of flow per fracture
Method of Moments		1.1 (Pe)	1200 (t_m)	190 (D)	2.1	1.
Sauty 1-D	241	30.4 (Pe)	90. (t_c)	280 (D)	9.7	1.
Sauty 2-D	240	30.2 (Pe)	93. (t_c)	270 (D)	9.4	1.
Single Fracture	290	4.04×10^{-4} (w)	(t_m)	830 (D)	10.	1.
Multifracture (model assumed three fractures)	74	3.69×10^{-2} (w_1) 753. (w_2) 24.1 (w_3)	66,200 (t_{m1}) 92. (t_{m2}) 20,500 (t_{m3})	390 (D_{Tr}) 1.40 (D_{Tr}) 0.19 (D_{Tr})	0.039 26. 0.12	0.76 0.19 0.05
Fracture-Matrix	219	2.17 (w)	52. (t_c)			1.
Double Porosity First Order Mass Transfer	283	0.13 (w)	56. (t_c)			1.
Double Porosity Slabs	257	14.5 (w)	77. (t_c)			1.
Double Porosity Cubes	271	11.2 (w)	75. (t_c)			1.

- 1 Pe = Peclet Number = uR/D or w = ratio of transport along the fracture to transport out of the fracture
- 2 t_c = transfer time by pure convection or the time that the pulse would reach the observation well if there is no diffusion
 t_m = mean residence time, as determined by first moment analysis
- 3 D = effective dispersion coefficient = uR/Pe or D_{Tr} = Taylor dispersion coefficient

Table 5.8 Comparison of All Models for BCF Inoculated into VM302D						
	Sum of Square Residuals ($\mu\text{g/L}$) ²	Characteristic Dimensionless Number ¹ Pe or w	Characteristic Time ² (min)	Effective Dispersion Coefficient ³ (cm^2/sec)	Average Radial Velocity (cm/min)	Fraction of flow per fracture
Method of Moments		2.9 (Pe)	2400 (t_m)	1.40 (D)	0.10	1.
Sauty 1-D	0.39	6.2 (Pe)	2300 (t_c)	6.8 (D)	1.1	1.
Sauty 2-D	0.44	5.9 (Pe)	2700 (t_c)	6.1 (D)	0.9	1.
Single Fracture	0.49	2.6×10^{-3} (w)	14,000 (t_m)	74. (D)	0.17	1.
Multifracture (model assumed three fractures)	0.40	0.13 (w_1) 5.5 (w_2) 23. (w_3)	1100 (t_{m1}) 3200 (t_{m2}) 19,000 (t_{m3})	670 (D_{Tr}) 5.4 (D_{Tr}) 0.23 (D_{Tr})	2.2 0.75 0.13	0.10 0.86 0.04
Fracture-Matrix	1.67	0.10 (w)	250 (t_c)			1.
Double Porosity First Order Mass Transfer	1.29	2.6×10^{-3} (w)	760 (t_c)			1.
Double Porosity Slabs	1.53	0.17 (w)	360 (t_c)			1.
Double Porosity Cubes	1.54	0.16 (w)	350 (t_c)			1.

- 1 Pe = Peclet Number = uR/D or w = ratio of transport along the fracture to transport out of the fracture
- 2 t_c = transfer time by pure convection or the time that the pulse would reach the observation well is there is no diffusion
 t_m = mean residence time, as determined by first moment analysis
- 3 D = effective dispersion coefficient = uR/Pe or D_{Tr} = Taylor dispersion coefficient

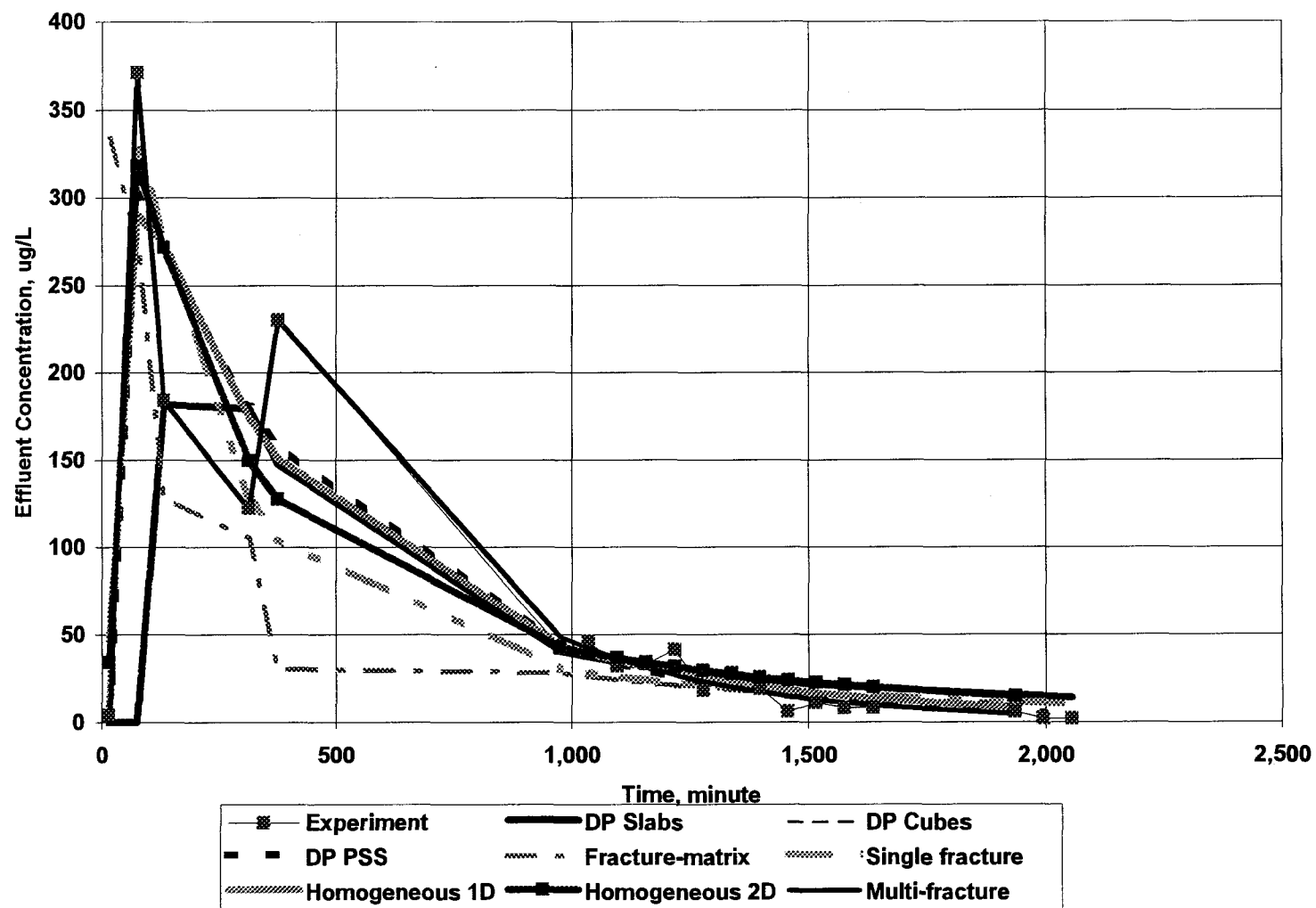


Figure 5.1 Breakthrough Curve and Modeled Results of PDMCB from P8M

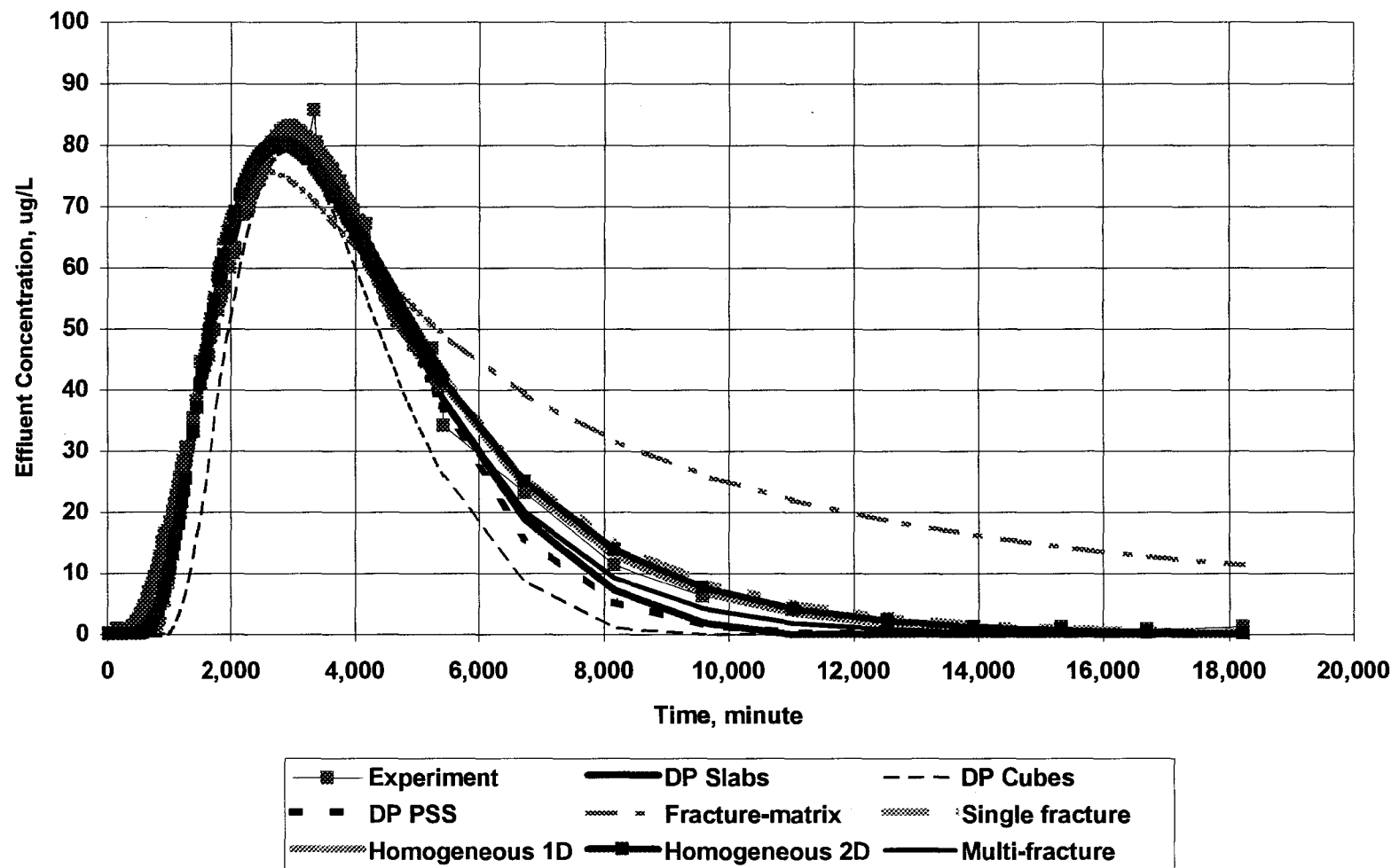


Figure 5.2 Breakthrough Curve and Modeled Results of PDMCB from VM302D

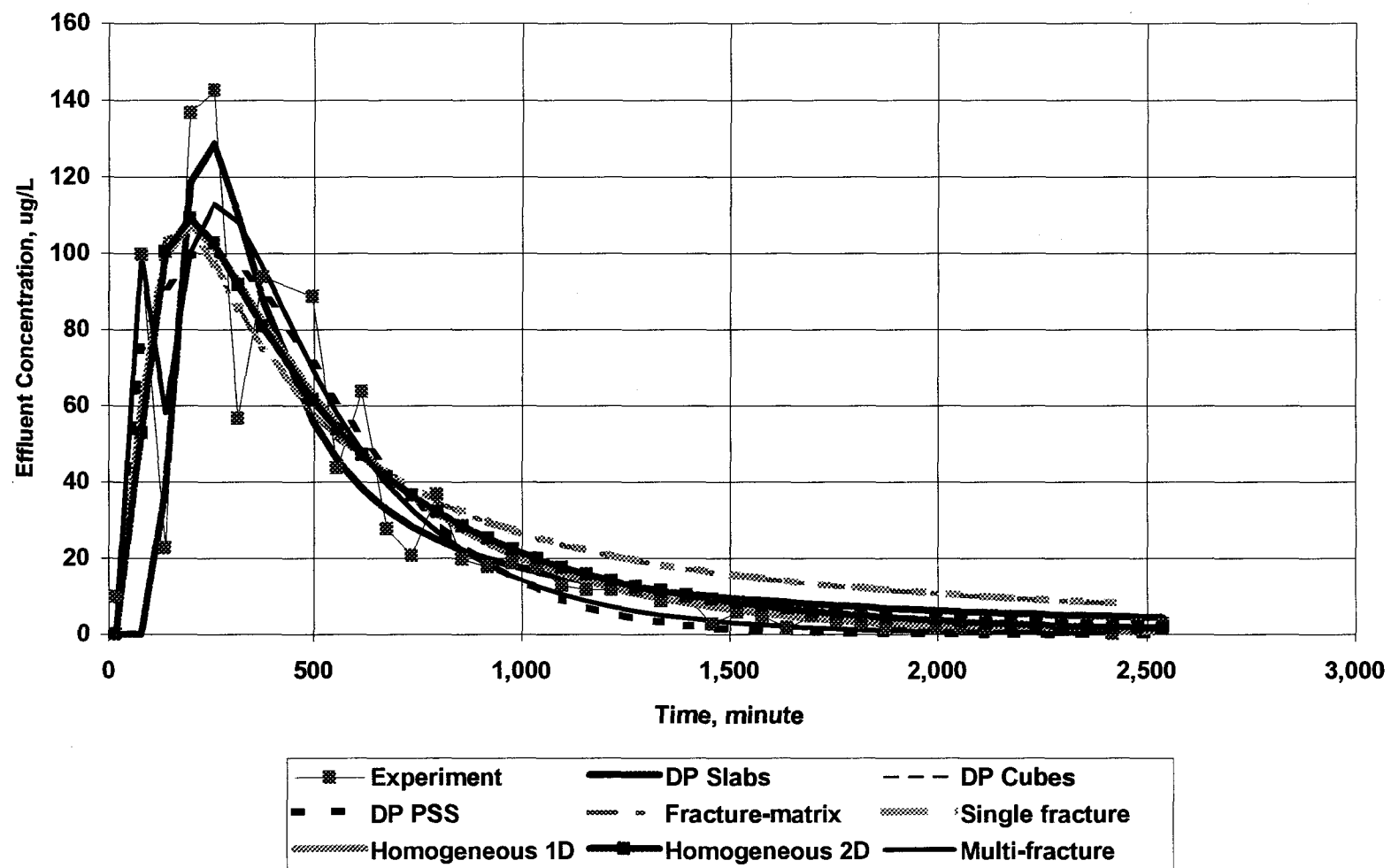


Figure 5.3 Breakthrough Curve and Modeled Results for Corrected Ethane from P8M

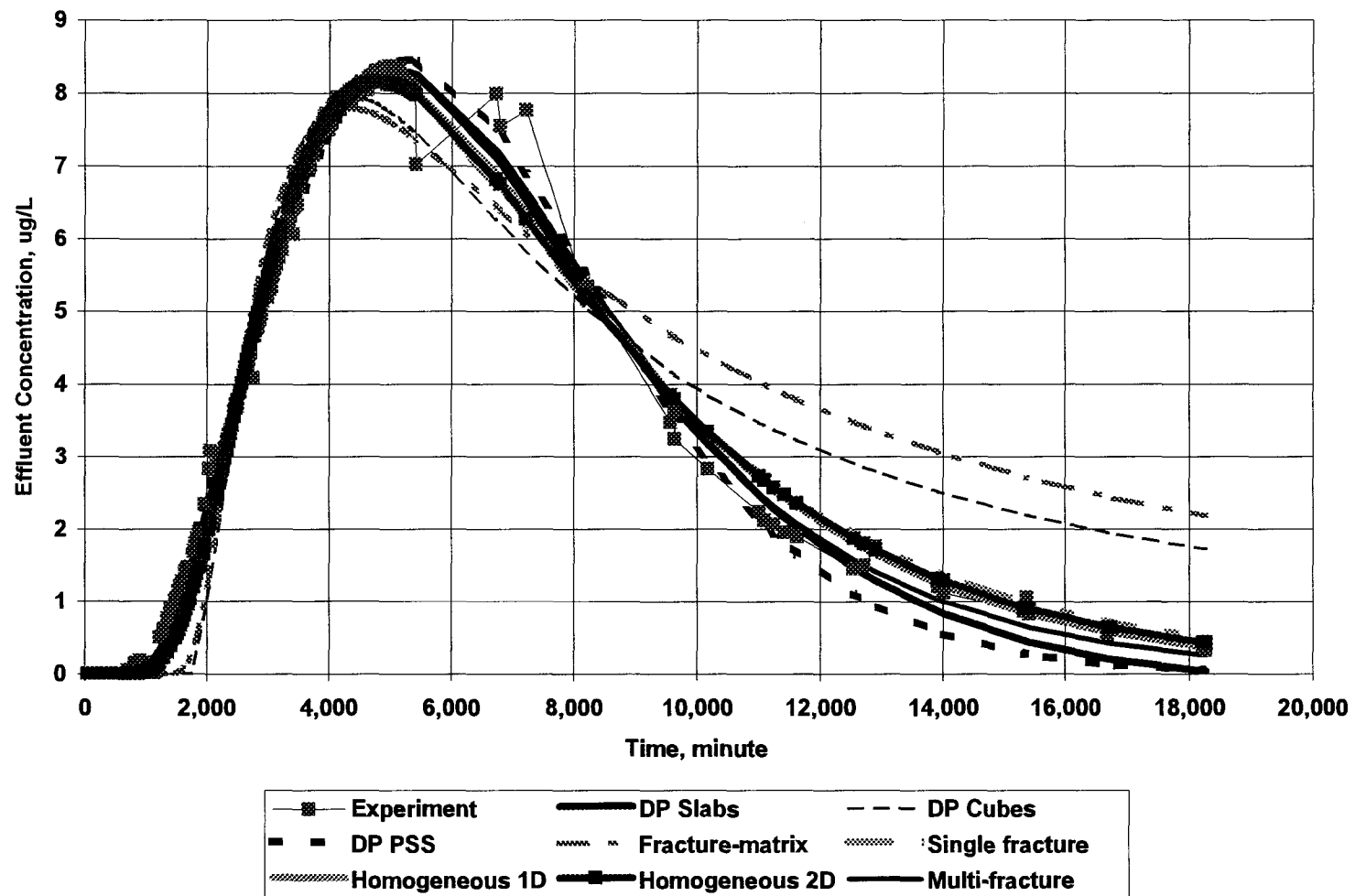


Figure 5.4 Breakthrough Curve and Modeled Results from Corrected Ethane from VM302D

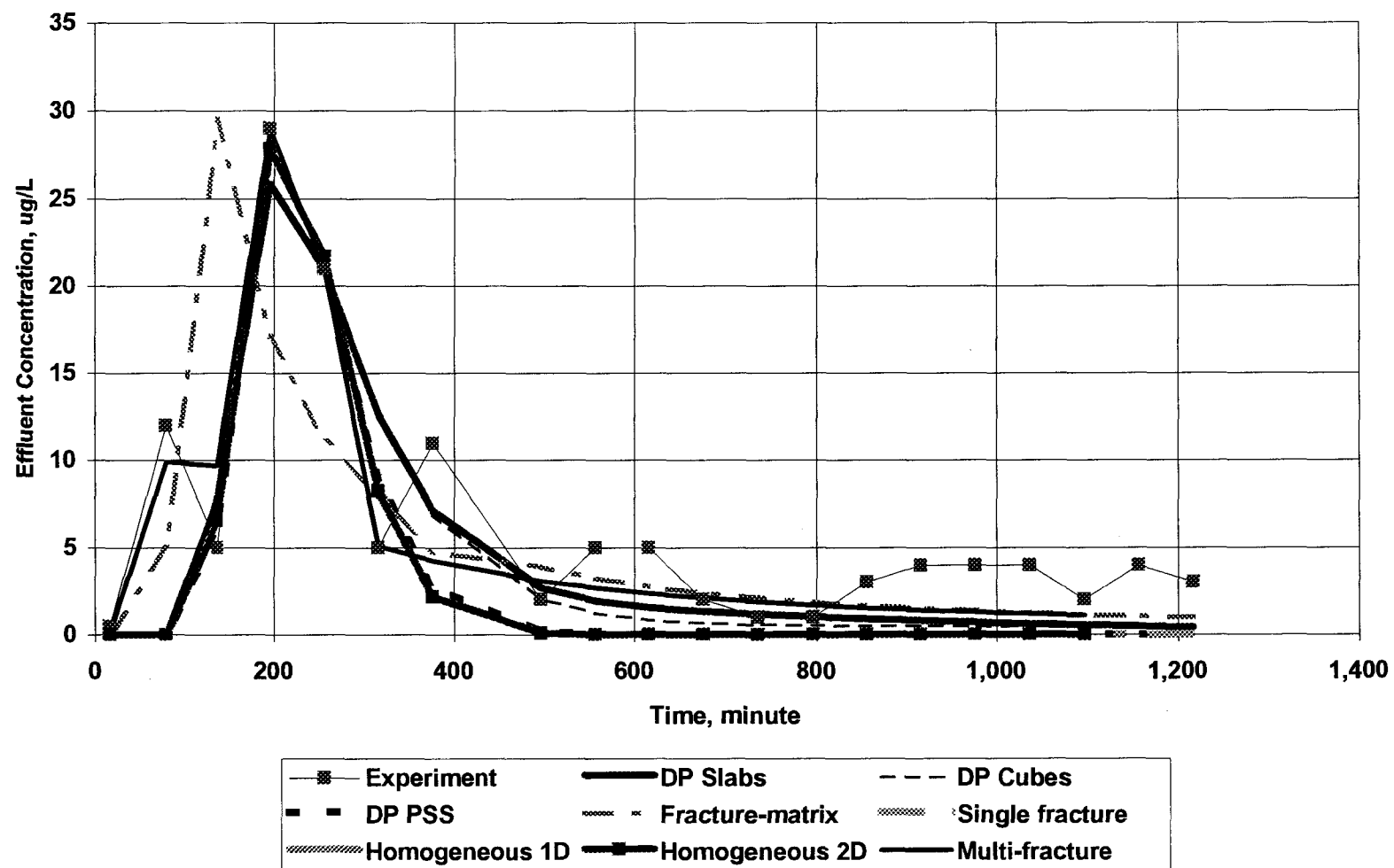


Figure 5.5 Breakthrough Curve and Modeled Results of BCF from TIA P8M

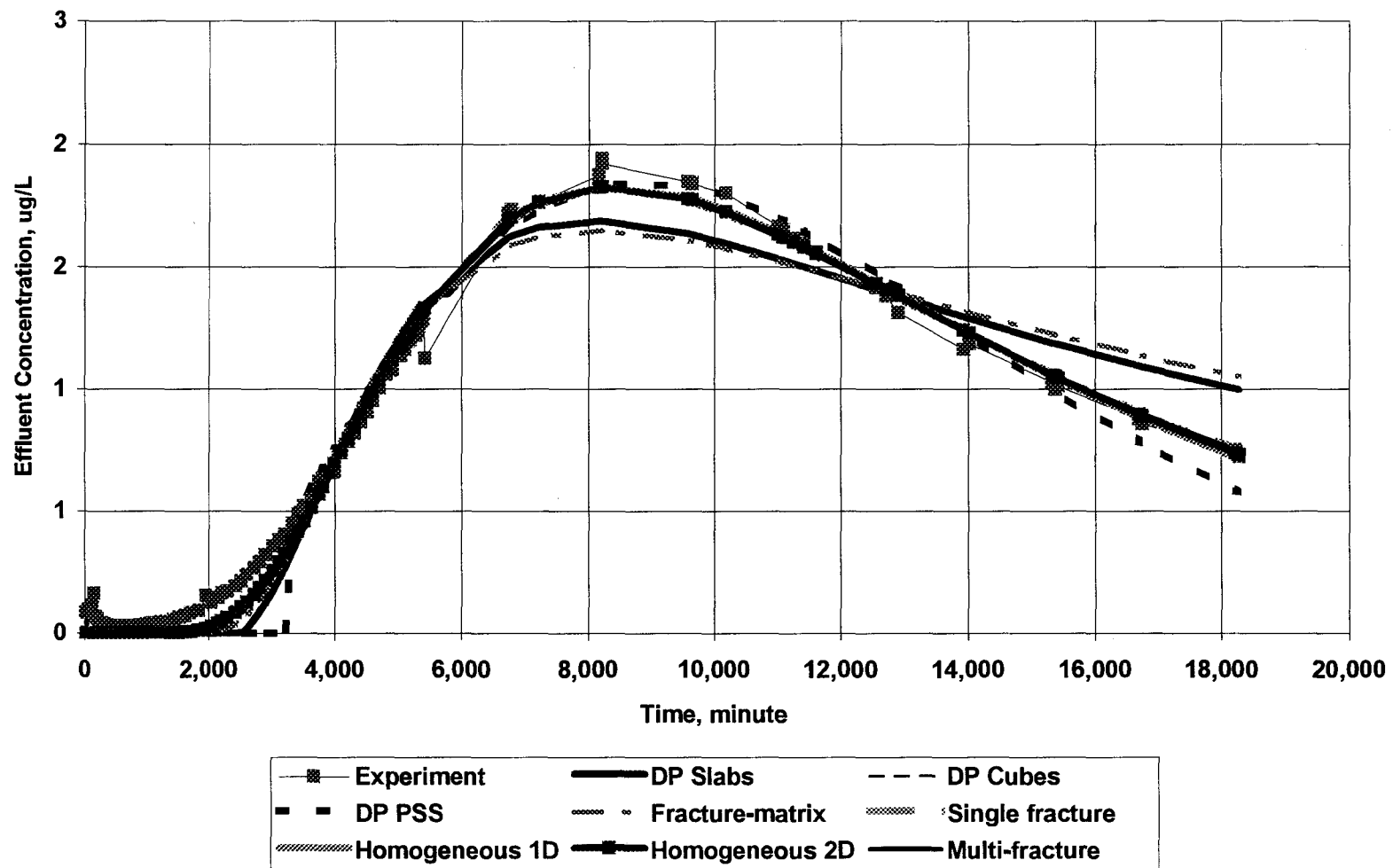


Figure 5.6 Breakthrough Curve and Modeled Results for BCF from VM302D

CHAPTER 6. CONCLUSIONS

Accurate knowledge of the existence and quantity of non-aqueous phase liquid (NAPL) present in the subsurface can assist in environmental remediation, optimization and closure. Superfund closure criteria depend on the ability to model contaminant mass flux into the groundwater. In a partitioning tracer test (PTT), a pulse containing one or more tracers is injected into the subsurface and effluent samples are collected from a distant extraction well. The effluent samples are analyzed for tracer concentrations. If one compound preferentially separates from the flowing stream into an immobile, immiscible liquid, then its arrival at the extraction point is delayed. The magnitude of this delay has been correlated to the amount of immiscible liquid present. While it is more common to perform partitioning tracer tests in the saturated zone, this work is one of the first gas-phase PTTs conducted in the vadose zone.

The objective of first component of this work was to identify gas-phase partitioning tracers and measuring their partitioning coefficients. In the vadose zone there are three phases present: NAPL, water, and air. Therefore, there are at least three types of tracers necessary: a nonreactive tracer such as a noble gas; a NAPL partitioning tracer, such as a perfluoride; and water partitioning tracer, such as a halon. Helium was employed as a nonpartitioning tracer. The perfluorides that were used in this test were perfluorodimethylcyclobutane, perfluorocyclopentane and perfluorocyclohexane. The

halons were bromochlorodifluoromethane, dibromodifluoromethane and dibromotetrafluoroethane. Additionally, this project used a fourth type of gas-phase tracer - the alkanes, methane and ethane. The alkanes had been used as nonreactive tracers in prior column tests and subsequently used in other field-scale gas-phase partitioning tests as nonpartitioning tracers. Therefore, they were expected to be nonpartitioning tracers for this work.

It was necessary to measure these tracers' NAPL-air and water-air partitioning coefficients. A laboratory method for measuring NAPL-air partitioning coefficients was developed. The measured NAPL-air partitioning of the halons indicated that they were so strongly NAPL-partitioning that their water partitioning characteristics, although measurable, were of less significance. The alkanes were unexpectedly found to be more retarded than the perfluoride tracers. The water content was determined by the alkane tracers for this work and not the halons.

The second component of this study involved conducting a field-scale gas-phase partitioning tracer test, and the results of which were used to estimate NAPL, water and air saturations. Three suites of three tracers were injected into three wells 14.5 to 24 m distant from a single extraction well. The nine tracer concentrations were determined in the effluent from the extraction well. The NAPL saturation was calculated to be an extremely low value (0.00071). Additionally, the water saturation for this project was

estimated to be approximately 90%, which is unexpectedly high for a vadose zone. The mass of NAPL present in the system was estimated to be 22,000 kg based on the PTT results. This value is in the same order as the amount of contaminant mass (28,600 kg) that has been removed via SVE.

In addition, the PTT and accompanying soil vapor extraction pilot test led to additional formation characterization. The vacuum response time indicated high formation permeability (10^{-12} m²). The rapid tracer response time, geological data, vacuum response and low effective formation porosity indicated that the formation is fractured. This work is one of the few PTTs conducted in heterogeneous media.

The third component of this work was to analyze the experimental data with simple mathematical models to determine transport parameters. Of those tested, two porous, three double porosity, and three fracture based (fracture matrix, single fracture, and multifracture) models could reasonably match the experimental data and no one model was consistently superior to the others. All of the models tended to under predict the concentrations at early times while overpredicting the tailing concentrations.

Different models determined different parameters and so a specific model should be selected based on the transport parameter that one wishes to determine. The porous media models can adequately predict mean arrival times, mean effective porosity values

and effective dispersivities. The fracture models were necessary to determine first tracer arrival times which would be necessary for conservative determination of possible contaminant presence for vapor intrusion modeling.

While all of the models tested were relatively simple, the more complex models (e.g., the two-dimensional porous versus the one-dimensional porous or the multi-fracture versus the single fracture) did not give superior results compared to the more simplistic counterparts. This work established that it is possible to determine field-scale formation and transport parameters through analysis of PTT tests, vacuum data, and geological data. Matching tracer data with simple models can generate field-scale transport parameter values. Modeling contaminant transport via simple models and field-scale parameter values could replace complicated three-dimensional numerical modeling and the necessary site characterization requirements.

REFERENCES

- Air Force, U. S., and Company, R. S. (2004). "Environmental Remediation Monthly Report."
- Akin, S. (2001). "Analysis of tracer tests with simple spreadsheet models." *Computers & Geosciences*, 27(2), 171-178.
- Annable, M. D., Jawitz, J. W., Rao, P. S. C., Dai, D. P., Kim, H., and Wood, A. L. (1998a). "Field evaluation of interfacial and partitioning tracers for characterization of effective NAPL-water contact areas." *Ground Water*, 36(3), 495-502.
- Annable, M. D., Rao, P. S. C., Hatfield, K., Graham, W. D., Wood, A. L., and Enfield, C. G. (1998b). "Partitioning tracers for measuring residual NAPL: Field-scale test results." *Journal of Environmental Engineering-ASCE*, 124(6), 498-503.
- Ashworth, R., Howe, G. B., Mullins, M. E., and Rogers, T. N. (1988). "Air-Water Partitioning Coefficients of Organics in Dilute Aqueous Solutions." *Journal of Hazardous Materials*, 18, 25-36.

- Baehr, A. L., and Hult, M. F. (1991). "Evaluation of insaturated zone air permeability through pneumatic tests." *Water Resources Research*, 27(10), 2605-2617.
- Barker, J. A. (1982). "Laplace transform solutions for solute transport in fissured aquifers." *Advances in Water Resources*, 5, 98-104.
- Bear, J., Tsang, C.-F., and Marsily, G. d. (1993). *Flow and contaminant transport in fractured rock*, Academic Press.
- Becker, M. W., and Charbeneau, R. J. (2000). "First-passage-time transfer functions for groundwater tracer tests conducted in radially convergent flow (vol 40, pg 299, 2000)." *Journal of Contaminant Hydrology*, 45(3-4), 359-+.
- Bem, H., Olszewski, M., and Kaczmarek, A. (2004). "Concentration of selected natural radionuclides in the thermal groundwater of Uniejow, Poland." *Nukleonika*, 49(1), 1-5.
- Bogdanov, I. I., Mourzenko, V. V., Thovert, J. F., and Adler, P. M. (2003a). "Effective permeability of fractured porous media in steady state flow." *Water Resources Research*, 39(1).

- Bogdanov, I. I., Mourenko, V. V., Thovert, J.-F., and Adler, P. M. (2003b). "Pressure drawdown well tests in fractured porous media." *Water Resources Research*, 39(1), 1021.
- Bodvarsson, G., and Tsang, C. F. (1982). "Injection and thermal breakthrough in fractured geothermal rocks." *Journal of Geophysical Research*, 87(B2), 1031-1048.
- Bodvarsson, G. S., Kwicklis, E., Shan, C., and Wu, Y. S. (2003). "Estimation of percolation flux from borehole temperature data at Yucca Mountain, Nevada." *Journal of Contaminant Hydrology*, 62-3, 3-22.
- Brusseau, M. L. (1992). "Rate-Limited Mass-Transfer and Transport of Organic Solutes in Porous-Media That Contain Immobile Immiscible Organic Liquid." *Water Resources Research*, 28(1), 33-45.
- Brusseau, M. L. (1997). "Interim Progress Report - Tucson International Airport." University of Arizona, Tuscon, AZ.
- Brusseau, M. L., Popovicova, J., and Silva, J. A. K. (1997). "Characterizing gas-water interfacial and bulk water partitioning for gas phase transport of organic contaminants in unsaturated porous media." *Environmental Science &*

Technology, 31(6), 1645-1649.

Brusseau, M. L. (1998). "Non-ideal transport of reactive solutes in heterogeneous porous media: 3. model testing and data analysis using calibration versus prediction."

Journal of Hydrology, 209(1-4), 147-165.

Brusseau, M. L., Bronson, K. M., Ross, S., and Nelson, N., T. (2003a). "Application of Gas-phase Partitioning Tracer Tests to Characterize Immiscible-liquid Contamination in the Vadose Zone Beneath a Fuel Depot." *Vadose Zone Journal*, 2, 148-153.

Brusseau, M. L., Nelson, N., T., and Constanza-Robinson, M. S. (2003b). "Partitioning Tracer Tests for Characterizing Immiscible-Fluid Saturations and Interfacial Areas in the Vadose Zone." *Vadose Zone Journal*, 2, 138-147.

Brusseau, M. L., Popovicova, J., and Silva, J. A. K. (1997). "Characterizing gas-water interfacial and bulk water partitioning for gas phase transport of organic contaminants in unsaturated porous media." *Environmental Science & Technology*, 31(6), 1645-1649.

Bullivant, D. P., and O'Sullivan, M. J. (1989). "Matching a Field Tracer Test With Some

Simple-Models." *Water Resources Research*, 25(8), 1879-1891.

Cain, R. B., Johnson, G. R., McCray, J. E., Blanford, W. J., and Brusseau, M. L. (2000).

"Partitioning tracer tests for evaluating remediation performance." *Ground Water*, 38(5), 752-761.

Carlson, T. D., Costanza-Robinson, M. S., Keller, J., Wierenga, P. J., and Brusseau, M.

L. (2003). "Intermediate-scale tests of the gas-phase partitioning tracer method for measuring soil-water content." *Soil Science Society of America Journal*, 67(2), 483-486.

Coats, K. H., and Smith, B. D. (1964). "Dead-End Pore Volume and Dispersion in Porous

Media." *Society of Petroleum Engineers Journal*, 4, 73-84.

Costanza, M. S., and Brusseau, M. L. (2000). "Contaminant vapor adsorption at the gas-

water interface in soils." *Environmental Science & Technology*, 34(1), 1-11.

Costanza-Robinson, M. S. (2001). "Elucidation of Retention Processes Governing the

Transport of Volatile Organic Compounds in Unsaturated Soils," Dissertation, University of Arizona, Tucson, AZ.

- Davis, B. M., Istok, J. D., and Semprini, L. (2002). "Push-pull partitioning tracer tests using Radon-222 to quantify non-aqueous phase liquid contamination." *Journal of Contaminant Hydrology*, 58, 129-146.
- Deans, H. A. (1978). "Using Chemical Tracers to Measure Fractional Flow and Saturation In-Situ." *Proceedings of the Fifth Symposium of Improved Methods of Oil Recovery*, SPE 7076.
- Deeds, N. E. (1999). "Development and Evaluation of Partitioning Interwell Tracer Test Technology for Detection of Non-Aqueous Phase Liquids in Fractured Media," Dissertation, University of Texas, Austin, TX.
- Deeds, N. E., McKinney, D. C., Pope, G. A., and Whitley, G. A. (1999a). "Difluoromethane as partitioning tracer to estimate vadose water saturations." *Journal of Environmental Engineering-Asce*, 125(7), 630-633.
- Deeds, N. E., Pope, G. A., and McKinney, D. C. (1999b). "Vadose zone characterization at a contaminated field site using partitioning interwell tracer technology." *Environmental Science & Technology*, 33(16), 2745-2751.
- Dobson, P. F., Kneafsey, T. J., Sonnenthal, E. L., Spycher, N., and Apps, J. A. (2003).

"Experimental and numerical simulation of dissolution and precipitation: implications for fracture sealing at Yucca Mountain, Nevada." *Journal of Contaminant Hydrology*, 62-3, 459-476.

Dugan, P. J., McCray, J. E., and Thyne, G. D. (2003). "Influence of a solubility-enhancing agent (cyclodextrin) on NAPL-water partition coefficients, with implications for partitioning tracer tests - art. no. 1123." *Water Resources Research*, 39(5), 1123-1123.

Dwarakanath, V., Deeds, N., and Pope, G. A. (1999). "Analysis of partitioning interwell tracer tests." *Environmental Science & Technology*, 33(21), 3829-3836.

Earlougher, R. C. (1977). *Advances in well test analysis*, Society of Petroleum Engineers of AIME, New York.

Falta, R. W. (1996). "A program for analyzing transient and steady-state soil gas pump tests." *Ground Water*, 34(4), 750-755.

Falta, R. W., Lee, C. M., Brame, S. E., Roeder, E., Coates, J. T., Wright, C., Wood, A. L., and Enfield, C. G. (1999). "Field test of high molecular weight alcohol flushing for subsurface nonaqueous phase liquid remediation." *Water Resources Research*,

35(7), 2095-2108.

Fetter, C. W. (1993). *Contaminant Hydrogeology*, Macmillan, New York.

Fossum, M. P., and Horne, R. N. (1982). "Interpretation of tracer return profiles at Wairakei geothermal field using fracture analysis." *Geothermal Resources Council Transactions*, 6, 261-264.

Freeze, R. A., and Cherry, J. A. (1979). *Groundwater*, Prentice-Hall, Inc., Englewood Cliffs, NJ 07632.

Gossett, J. M. (1987). "Measurement of Henry's Law Constants for C1 and C2 Chlorinated Hydrocarbons." *Environmental Science & Technology*, 21, 202-208.

Himmelblau, D. M., and Bischoff, K. B. (1968). *Process Analysis and Simulation*, John Wiley & Sons, New York.

Hinds, J. J., Ge, S. M., and Fridrich, C. J. (1999). "Numerical modeling of perched water under Yucca Mountain, Nevada." *Ground Water*, 37(4), 498-504.

Hine, J., and Mookerjee, P. K. (1975). "Structural effects on rates and equilibriums. XIX.

Intrinsic hydrophilic character of organic compounds. Correlations in terms of structural contributions." *Journal of Organic Chemistry*, 40, 292-298.

Horne, R. N. (1995). *Modern Well Test Analysis: A Computer-Aided Approach, Second Edition*, Petroway, Palo Alto, CA.

Horne, R. N., and Rodriguez, F. (1983). "Dispersion in tracer flows in fractured geothermal systems." *Geophysical Research Letters*, 10(4), 289-292.

Huang, K., Tsang, Y. W., and Bodvarsson, G. S. (1999). "Simultaneous inversion of air-injection tests in fractured unsaturated tuff at Yucca Mountain." *Water Resources Research*, 35(8), 2375-2386.

Hunt, T. M. (1998). "Recent developments in the New Zealand geothermal industry." *Energy Sources*, 20(8), 777-786.

Jensen, C. L., and Horne, R. N. (1983). "Matrix diffusion and its effect on the modeling of tracer returns from the fractured geothermal reservoir at Wairakei, New Zealand." *Proceedings Ninth Workshop on Geothermal Reservoir Engineering, Stanford University, Stanford, CA, December 13-15.*

- Jin, M. Q., Delshad, M., Dwarakanath, V., McKinney, D. C., Pope, G. A., Sepehrmoori, K., Tilburg, C. E., and Jackson, R. E. (1995). "Partitioning Tracer Test For Detection, Estimation, and Remediation Performance Assessment of Subsurface Nonaqueous Phase Liquids." *Water Resources Research*, 31(5), 1201-1211.
- Jin, M., Butler, G. W., Jackson, R. E., Mariner, P. E., Pickens, J. F., Pope, G. A., Brown, C. L., and McKinney, D. C. (1997). "Sensitivity models and design protocol for partitioning tracer tests in alluvial aquifers." *Ground Water*, 35(6), 964-972.
- Johnson, G. R., Gupta, K., Putz, D. K., Hu, Q., and Brusseau, M. L. (2003). "The effect of local-scale physical heterogeneity and nonlinear, rate-limited sorption/desorption on contaminant transport in porous media." *Journal of Contaminant Hydrology*, 64(1-2), 35-58.
- Joss, C. J., and Baehr, A. L. (1997). "Documentation of AIR2D, a computer program to simulate two-dimensional axisymmetric air flow in the unsaturated zone." United States Geological Survey, West Trenton, NJ.
- Karickhoff, S. W. (1984). "Organic pollutant sorption in aquatic systems." *Journal of Hydraulic Engineering*, 110(6), 707-35.

- Keller, J. M., and Brusseau, M. L. (2003). "In-situ characterization of soil-water content using gas-phase partitioning tracer tests: Field-scale evaluation." *Environmental Science & Technology*, 37(14), 3141-3144.
- Khutorskoi, M. D., Anitpov, M. P., Volozh, Y. A., and Polyak, B. G. (2004). "Temperature field and a 3D geothermal model of the North Caspian Basin." *Geotectonics*, 38(1), 53-60.
- Kim, H., Annable, M. D., and Rao, P. S. C. (2001). "Gaseous transport of volatile organic chemicals in unsaturated porous media: Effect of water-partitioning and air-water interfacial adsorption." *Environmental Science & Technology*, 35(22), 4457-4462.
- Kram, M. L., Keller, A. A., Rossabi, J., and Everett, L. G. (2001). "DNAPL characterization methods and approaches, part 1: Performance comparisons." *Ground Water Monitoring and Remediation*, 21(4), 109-123.
- Kram, M. L., Keller, A. A., Rossabi, J., and Everett, L. G. (2002). "DNAPL characterization methods and approaches, part 2: Cost comparisons." *Ground Water Monitoring and Remediation*, 22(1), 46-61.
- Kreft, A., and Zuber, A. (1978). "On the physical meaning of the disperiosn equation and

its solutions for different initial and boundary conditions." *Chemical Engineering Science*, 33, 1471-1480.

Lai, C. H., Bodvarsson, G. S., Tsang, C. F., and Witherspoon, P. A. "A new model for well test data analysis for naturally fractured reservoirs." *1983 California Regional Meeting of the Society of Petroleum Engineers*, Ventura, CA, 23-25.

Levenspiel, O. (1972). *Chemical Reaction Engineering*, John Wiley & Sons, New York, NY.

Lyman, W. J., Reehl, W. F., and Rosenblatt, D. H. (1990). *Handbook of chemical property estimation methods: environmental behavior of organic compounds*, American Chemical Society, Washington, DC.

Mackay, D., and Shiu, W. Y. (1981). "A Critical Review of Henry's Law Constants for Chemicals of Environmental Interest." *Journal of Physical and Chemical Reference Data*, 10(4), 1175-1199.

Maloszewski, P., and Zuber, A. (1985). "On the theory of tracer experiments in fissured rocks with a porous matrix." *Journal of Hydrology*, 79, 333-358.

- Mariner, P. E., Jin, M. Q., Studer, J. E., and Pope, G. A. (1999). "The first vadose zone partitioning interwell tracer test for nonaqueous phase liquid and water residual." *Environmental Science & Technology*, 33(16), 2825-2828.
- Meinardus, H. W., Dwarakanath, V., Ewing, J., Hirasaki, G. J., Jackson, R. E., Jin, M., Ginn, J. S., Londergan, J. T., Miller, C. A., and Pope, G. A. (2002). "Performance assessment of NAPL remediation in heterogeneous alluvium." *Journal of Contaminant Hydrology*, 54(3-4), 173-193.
- Montgomery, J. H. (1996). *Groundwater Chemicals Desk Reference - Second Edition*, CRC Lewis, Boca Raton.
- Mukhopadhyay, S., and Tsang, Y. W. (2002). "Understanding the anomalous temperature data from the Large Block Test at Yucca Mountain, Nevada - art. no. 1210." *Water Resources Research*, 38(10), 1210-1210.
- Nelson, N. T., and Brusseau, M. L. (1996). "Field study of the partitioning tracer method for detection of dense nonaqueous phase liquid in a trichloroethene-contaminated aquifer." *Environmental Science & Technology*, 30(9), 2859-2863.
- Nelson, N. T., Brusseau, M. L., Carlson, T. D., Costanza, M. S., Young, M. H., Johnson,

G. R., and Wierenga, P. J. (1999a). "A gas-phase partitioning tracer method for the in situ measurement of soil-water content." *Water Resources Research*, 35(12), 3699-3707.

Nelson, N. T., Oostrom, M., Wietsma, T. W., and Brusseau, M. L. (1999b). "Partitioning tracer method for the in situ measurement of DNAPL saturation: Influence of heterogeneity and sampling method." *Environmental Science & Technology*, 33(22), 4046-4053.

Parker, J. C., and van Genuchten, M. T. (1978). "Flux-averaged and volume-averaged concentrations in continuum approaches to solute transport." *Water Resources Research*, 20(7), 866-872.

Payne, T. H. (1999). "Quantifying Error in the Analysis of Partitioning Interwell Tracer Tests," Dissertation, Clemson University, Clemson, SC.

Peng, J., and Wan, A. (1997). "Measurement of Henry's Constants of High Volatility Organic Compounds Using a Headspace Autosampler." *Environmental Science & Technology*, 31(10), 2998-3003.

Popovicova, J., and Brusseau, M. L. (1994). "Transport of Gas-Phase Contaminants in the

Unsaturated Zone." *Abstracts of Papers of the American Chemical Society*, 207, 219-ENVR.

Rao, P. S. C., Annable, M. D., Sillan, R. K., Dai, D. P., Hatfield, K., Graham, W. D., Wood, A. L., and Enfield, C. G. (1997). "Field-scale evaluation of in situ cosolvent flushing for enhanced aquifer remediation." *Water Resources Research*, 33(12), 2673-2686.

Rasmuson, A. (1984). "Migration of radionuclides in fissured rock: Analytical solutions for the case of constant sources strength." *Water Resources Research*, 20(10), 1435-1442.

Rasmuson, A., and Neretnieks, I. (1981). "Migration of radionuclides in fissured rock: The influence of micropore diffusion and longitudinal dispersion." *Journal of Geophysical Research*, 86(B5), 3749-3758.

Raven, K. G., Novakowaki, K. S., and Lapcevi, P. A. (1988). "Interpretation of Field Tracer Tests of a Single Fracture Using a Transient Solute Storage Model." *Water Resources Research*, 24(12), 2019-2032.

Sauty, J.-P. (1978). "Identification des parameters du transport hydrodispersif des les

aquiferes par interpretation de traces en ecoulement cylindrique convergent and divergent." *Journal of Hydrology*, 39(1/2), 69-103.

Sauty, J.-P. (1980). "An analysis of hydrodispersive transfer in aquifers." *Water Resources Research*, 16(1), 145-158.

Semprini, L., Hopkins, O. S., and Tasker, B. R. (2000). "Laboratory, field and modeling studies of radon-222 as a natural tracer for monitoring NAPL contamination." *Transport in Porous Media*, 38(1-2), 223-240.

Senum, G. I., Fajer, R., DeRose, W. E., Harris, J., B.R., Ottaviani, W. L., and (1992). "Petroleum Reservoir Characterization by Perfluorocarbon Tracers." *SPE/DOE Eighth Symposium on Enhanced Oil Recovery*, Tulsa, OK, 337-344.

Simon, M. A., Brusseau, M. A., Golding, R., and Cagnetta, P. J. (1998). "Vadose zone characterization at a contaminated field site using partitioning interwell tracer technology." *Platform Abstracts of the First International Conference on Remediation of Chlorinated and Recalcitrant Compounds*.

Stehfast, H. (1970). "Algorithm 368 Numerical Inversion of Laplace Transform." *Communications of the ACM*, 13(1), 47-49.

- Sudicky, E. A., and Frind, E. O. (1982). "Contaminant transport in fractured porous media: Analytical solutions for a system of parallel fractures." *Water Resources Research*, 18(6), 1634-1642.
- Tang, J. S. (1992). "Interwell Tracer Tests to Determine Residual Oil Saturation to Waterflood At Judy Creek BHL "A" Pool." *Journal of Canadian Petroleum Technology*, 31(8), 61-71.
- Tang, J. S., and Harker, B. (1991). "Interwell Tracer Test to Determine Residual Oil Saturation in a Gas-Saturated Reservoir .2. Field Applications." *Journal of Canadian Petroleum Technology*, 30(4), 34-42.
- Taylor, G. (1953). "Dispersion of soluble matter in solvent slowly through a tube." *Proceedings of Royal Society of London. Series A, Mathematical and Physical Sciences*, 219(1137), 186-203.
- Tsang, Y. W. (1992). "Usage of "Equivalent Apertures" for Rock Fractures as Derived From Hydraulic and Tracer Tests." *Water Resources Research*, 28(5), 1451-1455.
- Toride, N., Leij, F. J., and van Genuchten, M. T. (1995). "The CXTFIT Code for Estimating Transport Parameters from Laboratory Research Report No. 137."

United States Salinity Laboratory, Riverside, CA.

van Swaaij, W. P. M., Charpentier, J. C., and Villermaux, J. (1969). "Residence time distribution in the liquid phase of trickle flow in packed columns." *Chemical Engineering Science*, 24, 1083-1095.

Villermaux, J., and van Swaaij, W. P. M. (1969). "Modèle représentatif de la distribution des temps de séjour dans un réacteur semi-infini à dispersion axiale avec stagnantes. Application à l'écoulement ruisselant dans des colonnes d'anneaux Raschig." *Chemical Engineering Science*, 24, 1097-1111.

Vulava, V. M., Perry, E. B., Romanek, C. S., and Seaman, J. C. (2002). "Dissolved gases as partitioning tracers for determination of hydrogeological parameters." *Environmental Science & Technology*, 36(2), 254-262.

Warren, J. E., and Root, P. J. (1963). "The behavior of naturally fractured reservoirs." *Society of Petroleum Engineers Journal*, 245-255.

Werner, D., and Hohener, P. (2002). "Diffusive partitioning tracer test for nonaqueous phase liquid (NAPL) detection in the vadose zone." *Environmental Science & Technology*, 36(7), 1592-1599.

- Whitley, G. A. (1997). "An Investigation of Partitioning Tracers for Characterization of Nonaqueous Phase Liquids in Vadose Zones," Dissertation, The University of Texas at Austin, Austin, Texas.
- Whitley, G. A., McKinney, D. C., Pope, G. A., Rouse, B. A., and Deeds, N. E. (1999). "Contaminated vadose zone characterization using partitioning gas tracers." *Journal of Environmental Engineering-Asce*, 125(6), 574-582.
- Wilson, R. D., and Mackay, D. M. (1995). "Direct-Detection of Residual Nonaqueous Phase Liquid in the Saturated Zone Using SF₆ As a Partitioning Tracer." *Environmental Science & Technology*, 29(5), 1255-1258.
- Wood, M., Simmons, C. T., and Hutson, J. L. (2004). "A breakthrough curve analysis of unstable density-driven flow and transport in homogeneous porous media - art. no. W03505." *Water Resources Research*, 40(3), 3505-3505.
- Wörman, A., Xu, S. L., and Dverstorp, B. (2003). "Kinematic analysis of solute mass flows in rock fractures with spatially random parameters." *Journal of Contaminant Hydrology*, 60(3-4), 163-191.
- Wu, Y. S., and Pruess, K. (2000). "Numerical simulation of non-isothermal multiphase

tracer transport in heterogeneous fractured porous media." *Advances in Water Resources*, 23(7), 699-723.

Zhang, Y., and Graham, W. D. (2001). "Spatial characterization of a hydrogeochemically heterogeneous aquifer using partitioning tracers: Optimal estimation of aquifer parameters." *Water Resources Research*, 37(8), 2049-2063.